Submitted to Physical Review

UCRL-20075
Preprint

c.2

$\pi^- p$ REACTIONS AT 456, 505 AND 552 MeV/c

D. H. Saxon, J. H. Mulvey, and W. Chinowsky

October 1970

AEC Contract No. W-7405-eng-48

LAWRENCE RADIATION LABORATORY
UNIVERSITY of CALIFORNIA BERKELEY

UCRL-20075

DISCLAIMER

π^-p Reactions at 456, 505 and 552 MeV/c*

D.H. Saxon

and

J.H. Mulvey

Nuclear Physics Dept., Keble Road, Oxford

and

W. Chinowsky

Lawrence Radiation Laboratory, Berkeley, Calif. 94720.

* Work supported in part by the United Kingdom Science Research Council and in part by United States Atomic Energy Commission.

ABSTRACT

We present the results of an experiment to study the reactions $\pi^- p \rightarrow \pi\pi N$ at incident momenta of 456, 505 and 552 MeV/c in a hydrogen bubble chamber. The most prominent features of the data in the $\pi^+\pi^- n$ final state are a high-mass peak in the $M^2(\pi^+\pi^-)$ spectrum, (which moves upward in mass and becomes less significant as the incident momentum increases), and Δ^- production. We show that the $\pi^+\pi^-$ enhancement can be explained by the introduction of an $I = J = 0$ $\pi\pi$ interaction, and investigate two forms for this interaction. Within the framework of an isobar model, we derive values of the πN partial wave inelasticities and compare these with the predictions of πN elastic phase-shift analyses. It is shown that the branching ratio πN : $\pi\Delta$: σN of the P_{11} partial wave depends strongly on the assumed form of $\pi\pi$ final state interaction.

I. Introduction

This paper describes the analysis of new data on the reactions $\pi^- p \to \pi^- p$ and $\pi^- p \to \pi\pi N$ (chiefly $\pi^+\pi^- n$) at incident momenta of 456, 505, and 552 MeV/c.

In previous studies of these reactions at similar energies [1] [2] a broad enhancement was observed, at about 400 MeV/c^2, in the $\pi^+\pi^-$ mass spectrum which was absent in the $\pi^-\pi^0$ distribution. It has been a principal purpose of this experiment to obtain sufficient statistical accuracy to enable a detailed analysis of these final states to be made and to find an explanation of this effect. At the same time the analysis provides information, which was previously lacking, on the partial wave inelasticities and branching ratios of the πN system in the mass range 1338 to 1402 MeV/c^2. (Work in progress will extend the range to 1300 to 1520.) At these energies the only inelastic channels are to three-body final states, with consequent uncertainties in interpretation, owing to the need for a model if useful information is to be obtained. Pion-nucleon s-channel processes are expected to dominate at these low energies; there is no evidence of the presence of exchange mechanisms, and so they have not been considered in the analysis. The so-called "isobar model" [3] is used here.

In the model coherent production of $\pi\Delta$ and $N\sigma$ is assumed, where σ is an $I = J = 0$ state of two pions. The formulation of this model, and its inherent difficulties, are discussed in section IV. The data are described in section II; the elastic differential cross-section and

inelastic cross-section determination are dealt with in section II.2. Section III gives the results of a model-independent moments analysis. The isobar model is fitted to the data in section V. In section VI predictions are made of πN partial wave inelasticities and compared with those of elastic phase-shift analyses and in section VII the P_{11} branching ratio is calculated. Section VIII summarises the conclusions of this work.

II. Experimental details and data

II.1 The experiment

The Saclay 180 litre (80 cm) hydrogen bubble chamber was exposed to incident negative pions at the NIMROD accelerator of the Rutherford High Energy Laboratory in November 1966 and April 1967. In the exposure 145,000 pictures were taken at 456 Mev/c, 85,000 at 505 Mev/c and 45,000 at 552 Mev/c.

Especially at the lowest momentum, contamination of the beam with electrons and muons was a serious problem and to eliminate electrons in the run at 456 MeV/c a 1/8" Pb foil was put in the beam at an intermediate focus. A bending magnet removed degraded electrons from the beam before it entered the bubble chamber.

Scanning and measuring of the lower momenta film were done at Oxford University Nuclear Physics Laboratory; the 552 MeV/c exposure was processed at the Lawrence Radiation Laboratory, Berkeley. Measurements at both laboratories

were made with image plane digitisers having setting accuracy about seven microns on film.

The reactions giving rise to two-prong events are

$$\pi^- + p \rightarrow \pi^- + p \qquad (1)$$

$$\pi^- + p \rightarrow \pi^- + p + \pi^0 \qquad (2)$$

$$\pi^- + p \rightarrow \pi^- + \pi^+ + n \qquad (3)$$

Of these the elastic scattering (1) is most common and reaction (2) is the rarest, having only about one-fifth the number of events of reaction (3). The cross-section for four-prong events is very small (less than ten events seen), and contamination of reaction (2) by cases of $\pi^- p \pi^0 \pi^0$ is entirely negligible.

The film with the lower momenta incident pions was prescanned to select examples of the reaction $\pi^- p \rightarrow \pi^- \pi^+ n$ among the much more numerous elastic scatterings; criteria based on bubble density and curvature of the positive tracks readily permitted elimination of events with proton rather than π^+ tracks. In case of doubt the event was measured. In all such situations, kinematic identification of the tracks provided an unambiguous selection. Since it is not possible to select examples of $\pi^- p \rightarrow \pi^- \pi^0 p$ using only visual criteria and it was not feasible to measure all events ($\sim$ 20,000 at 505 MeV/c, $\sim$ 35,000 at 456 MeV/c) the data at these two momenta are restricted to the $\pi^- \pi^+ n$ channel and, in the 505 MeV/c data, a sample of other events randomly selected. This group includes elastic scatters and a small number of π^0 production events.

All events were measured in the film with 552 MeV/c incident pions. Those data contain events in both inelastic channels, as well as elastic scatters. Part of the film was scanned twice to provide a measure of the scanning efficiency for different classes of events. After eliminating events not satisfying incident track momentum and entrance angle criteria, those outside the chosen fiducial volume and with confidence level $< 1\%$, there resulted the numbers of events, in the various final states, listed in Table I. The 528 examples of $\pi^-\pi^0 p$, at the highest momentum, were selected using the standard techniques of selection based on consistency of the measured quantities with the appropriate kinematical constraints. In cases where the identification was ambiguous between an inelastic mode and an elastic, the event was assigned to the elastic category. These were small enough in number so that there is no significant contamination, or loss, of events in the $\pi^-\pi^0 p$ data [5]. No physically significant biases were discovered, in a thorough search, except in the elastic scattering data, in which extreme forward and backward scatters are sometimes difficult to see. The elastic scattering data in section II.2 are given after correction for scanning losses. The correction is reliable except for $\cos\bar{\theta} > 0.9$ ($\bar{\theta}$ is the scattering angle in the centre of mass). A fuller account of the experimental details is given elsewhere [6].

II.2 The Elastic Scattering and Cross-section Normalisation

In figures 1 and 2 the distributions in $\cos\bar{\theta}$ for elastic

scatters at the two higher momenta are shown [7].

To obtain total cross sections for inelastic reactions, we normalize to the elastic scattering differential cross sections of Ogden et al. [9]. This procedure is more reliable than incident beam track counting, first because of the unknown contamination of electrons and muons in the beam and second the relative scanning efficiencies can be evaluated better than the absolute.

The cross-section in the range $-0.9 < \cos\bar{\theta} < 0.5$, which is least affected by scanning losses and varies slowly with incident momentum, was interpolated between the Ogden data. The results are given in Table II. For information, we include the 456 MeV/c inelastic cross-sections from the compilation of Yodh [10]. Our values at the higher momenta are in excellent agreement with the data of this compilation.

II.3 The three-body final states

A two-to-three-body reaction is described in its centre-of-mass by five kinematic variables (ignoring spin). We choose a right-handed axis system in the final state, with the x-axis along the outgoing nucleon, and the z-axis along $\vec{p}_N \times \vec{p}_{\pi_1}$ where $\vec{p}_N$ and $\vec{p}_{\pi_1}$ are the outgoing momenta of the nucleon and π^+, in $\pi^+\pi^-n$, or π^- in $\pi^-\pi^0p$.

Five independent variables are

$s^{\frac{1}{2}}$, the centre-of-mass energy

m_{12} , the invariant mass of particles 1 and 2;

m_{23} , the invariant mass of particles 2 and 3;

$\cos\Theta$, where Θ is the polar angle of the incident π^- with respect to the axes described above;

Φ , the azimuthal angle of the incident π^-.

The angles have been used by previous authors [11] [12] [13] [14] [15] [16].

Other variables may also be defined, viz.

m_{13} = the invariant mass of particles 1 and 3, with

$$m_{12}^2 + m_{23}^2 + m_{13}^2 = s + m_1^2 + m_2^2 + m_3^2$$

and $\cos\bar{\theta}_1$, $\cos\bar{\theta}_2$, $\cos\bar{\theta}_3$, the cosines of the production angles of the three final-state particles. By production angle we mean the angle, in the centre-of-mass, between the directions of the incident π^- and the outgoing particle.

Figures 3, 4, and 5 show the Dalitz plots for the $\pi^-\pi^+n$ state at each of the three energies. At all energies a strong concentration is seen at large $\pi^-\pi^+$ effective mass and large π^-n effective mass. Projections on the Dalitz plot axes, the $\pi^+\pi^-$ and π^-n mass^2 distributions, and, for completeness, the π^+n mass^2 distributions, are shown in Figs. 7, 8, 11, and 12. The peaking at high $\pi^-\pi^+$ mass is evident at all three energies. The π^-n distribution shifts toward high masses at the higher momenta. These features of the mass spectra were already prominent in the early results of Kirz, Schwartz, and Tripp [1] and led to speculation about a

possible I = 0, J = 0 pion-pion resonant final-state interaction. A difficulty with this simple interpretation is that no clearly defined peak above a continuous background appears in the mass distributions. Indeed the maximum in the $\pi^-\pi^+$ mass spectrum moves with incident energy so that it is not possible to define a mass for the conjectured resonance. A more sophisticated formalism, including effects of both $\pi\pi$ and πN final state interactions, is required for a satisfactory interpretation of the data.

Figures 6, 7 and 8 show the 552 MeV/c $\pi^-\pi^0$p Dalitz plot and effective mass distributions. Compared to the $\pi^-\pi^+$n data, there appears considerably less evidence for final state interactions. Neither the $\pi\pi$ or π-N mass distributions show strong peaking. This indicates that any strong $\pi\pi$ interaction must be in the isotopic spin zero state. Differences among the pion-nucleon mass spectra in the two final states can be simply understood as a feature of the production of the Δ (1236) resonance. Isotopic spin conservation selection rules strongly favour production of the negatively charged isobar and so strongest peaking in the π^-n mass spectrum, as observed.

The distributions in the angles Θ and Φ the angles of the incident pion direction with respect to the "body-fixed" axes defined above, and the production angles, are shown in Figs. 9 to 12. Both the $\pi^-\pi^+$n and $\pi^-\pi^0$p data are presented. No strong departures from isotropy in the cos distributions are noted. However, the azimuthal angular distributions are strongly non-isotropic and unsymmetric, even at the lowest

energy of the $\pi^-\pi^+$n state. This non-isotropy is also present in the Φ distribution for the $\pi^-\pi^0$p data but is perhaps not as clearly established because of the severe statistical uncertainties. An immediate conclusion is that at least two angular momentum states of opposite parity contribute to the pion production.

The production angle distributions show no strong forward or backward peaking. This suggests that an s-channel model will be particularly simple and involve only a few partial waves. There is no reason to consider t-channel models.

III. Model independent analysis

Some indication of the magnitude of the various initial state angular momentum waves present may be inferred, independently of any dynamical assumptions, from the coefficients in an expansion of the production intensity in a series of spherical harmonics. With the variables Θ, Φ, $m_{\pi\pi}$, $m_{\pi N}$ used here, this is

$$W(\Theta, \Phi, m_{\pi\pi}, m_{\pi N}) = \sum_{K,M} \sqrt{\frac{2K+1}{4\pi}}\, W_K^M(m_{\pi\pi}, m_{\pi N}) Y_{KM}^*(\Theta, \Phi).$$

The expansion coefficients W_K^M are functions of position in the Dalitz plot. In principle, a good representation of the experimental results is provided by the dependence of these coefficients upon position in Dalitz plot. Also, differences in partial wave contributions to σ production and Δ production may be noted by the variation of these parameters from, for

instance, large $\pi\pi$ mass to large πN mass. Unfortunately the statistical uncertainties in restricted groupings of the data are too severe to permit conclusions, and so we only give the coefficients for the complete samples of data.

Table III gives the values of the W_K^M and their errors for $K \leq 5$. All higher moments are, within the errors, consistent with zero. Those moments not given may be determined from the relations

$$W_K^{-M} = (-1)^M \quad W_K^{M\,*}$$

$$W_K^M = 0 \quad \text{if } (K + M) \text{ is odd.}$$

The relationship between these coefficients and the partial wave amplitudes is not very transparent [11] [12] [13] [14]. Only qualitative conclusions about the contributing angular momentum amplitudes may be inferred from the values of these coefficients. It can be seen from Table IV, giving the confidence levels that particular moments are zero, that all W_K^M with $K = 1, 2$ are non-zero. The W_1^1 coefficient is a sum of products of initial state angular momentum wave amplitudes, with each term a product of opposite-parity amplitudes. Thus the inelastic reactions proceed from at least two initial-state states of opposite parity [17]. Only angular momentum states with $J \geq L + 1/2$ contribute to the W_{2L}^M moments. The maximum total angular momentum with significant amplitude may be obtained directly from the knowledge of the maximum value of K in the spherical harmonic series.

As can be seen from Tables III and IV, only those moments with $K \leq 4$ are significantly different from zero. There is therefore no need for both $D_{5/2}$ and $F_{5/2}$ waves. In subsequent analysis we have considered only waves of $J \leq 3/2$.

IV. The Isobar Model

IV.1 General remarks

Because of the low centre-of-mass energy, the natural formalism to consider is an s-channel partial wave analysis. The mass^2 spectra suggest that the $\pi^+\pi^-n$ final-state is dominated by Δ resonance production, and perhaps a $\pi\pi$ interaction. This situation suggests application of an "isobar model". If the two-particle to two-particle amplitude is dominated by resonances, (this is referred to as the "separable" approximation, since the transition amplitudes separate into a factor depending on the initial state only and one depending on the final state only,) then the two-to-three particle amplitude can be expanded in a series, which can be written diagrammatically as in figure 14. If one curtails the series at the first term one has the "isobar model" [18] [19] [20] [21].

The second-order "rescattering" graphs are usually small [22], except at low energies. Anisovich and Dakhno [23] have suggested that the high-mass $\pi^+\pi^-$ peak in $\pi^+\pi^-n$ is due to destructive interference of the rescattering and isobar terms at low $\pi^+\pi^-$ masses. Anisovich et al. [24] have fitted the data of Batusov et al. [25] with a series of terms, which include a $\pi\pi$ rescattering vertex but not $\pi\pi$ isobar production.

In this paper we fit the data using only the first-order (isobar) terms. Any residual discrepancies between the isobar model predictions and the data may be due to the rescattering terms.

In the formulation of the model used here, all angular momentum, isospin and interference effects are taken into account. Such models have been described by Deler and Valladas [15] and Namyslowski, Razmi and Roberts [26]. The formalism used here is conceptually similar to that of Deler and Valladas, and so details of the derivation are not given.

IV.2 Formulation of the Isobar Model

The production of an isobar of particles 1 and 2, with spin j_{12} and orbital angular momentum ℓ_{12} is described in an angular momentum base $|(12)\ 3\rangle$ [26] [27]. We quantise

ℓ_{12} = relative angular momentum of 1 and 2,

j_{12} = total angular momentum of 1 and 2,

L'_3 = relative angular momentum of 3 and the (12) system in the overall centre-of-mass and

J = total angular momentum [28].

The matrix element for production of a (12) isobar involves only one value of j_{12} and ℓ_{12}.

Production of a (13) isobar is described in terms of

$j_{13}\ \ell_{13}\ L'_2\ J$. This basis is not orthogonal to $j_{12}\ \ell_{12}\ L'_3\ J$. We are therefore 'double-counting' to some extent. The advantage of this scheme is that we simply make use of the isotopic spin relations between Δ^- production in the $|(\pi^-n)\pi^+\rangle$ basis and Δ^+ production in the $|(\pi^+n)\pi^-\rangle$ basis. The three-body production amplitude is then a sum of amplitudes for the three processes

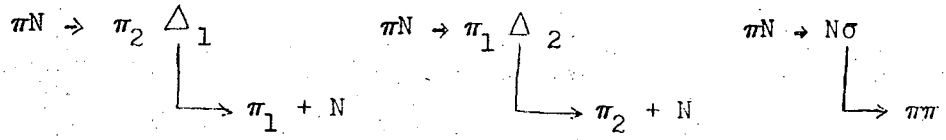

Including all kinematic factors within the definition of the matrix element the differential cross-section is

$$\frac{\partial^4\sigma}{\partial m_{12}^2\,\partial m_{23}^2\,\partial\cos\Theta\,\partial\Phi} = \frac{1}{2}\sum_{MM_S}\left|\sum_{JLL';I}\left\{T_I^{JLL'}\ (\pi\Delta_1) + T_I^{JLL'}\ (\pi\Delta_2)\right\} + \sum_{JLL'} T^{JLL'}\ (\sigma N)\right|^2$$

where the sum over final nucleon spin M_s and average over initial spin M are indicated. The axis of quantization in each case is the z-axis defined in section II.3. Each amplitude is to be understood as dependent upon M and M_s, though not explicitly indicated by the notation. Here $T_I^{JLL'}$ are the partial wave projections of the T-matrix for Δ-production in the state with total isotopic spin I. J and L' have the meanings above and L is the relative angular

momentum in the initial state. $T^{JLL'}$ are the amplitudes for production of an I = 0, J = 0 dipion isobar, σ, (see section IV.4) in the I = 1/2 state only.

IV.3 The $\pi\Delta$ Channel

We write the isospin decomposition of $\pi^- p \to \pi \Delta_1$

$$T_I^{JLL'}(\pi \Delta_1)$$

$$= C^{1\ \frac{1}{2}\ I}_{q_\pi\ q_N\ I_3}\ C^{1\ \frac{1}{2}\ 3/2}_{q_1\ q'_N\ q'_1}\ C^{1\ 3/2\ I}_{q_2\ q'_1\ I_3}\ T_I^{JLL'}(\pi\Delta)$$

where q_π, q_N and q'_N, are the 3rd components of isotopic spin of the incident π^-, initial and final nucleons and q_1, q_2 are the charges of final state pions 1 and 2, and Δ_1 is made of π_1 and N.

Factors containing the angular dependence of the $T_I^{JLL'}(\pi\Delta)$ are separated out as follows :

$$T^{JLL'}_{IMM_S}(\pi\Delta) = T_I^{JLL'}(s^{\frac{1}{2}}, m_\Delta)\ f^{JLL'}_{MM_S}(\Theta, \Phi, \phi_1, \theta^*)$$

where the suffices M and M_s have been reinserted. $T_I^{JLL'}(s^{\frac{1}{2}}, m_\Delta)$ is a reduced matrix element of the Breit-Wigner form for Δ final state interaction together with an angular momentum barrier for Δ-production at total c.m. energy $s^{\frac{1}{2}}$.

The form used here is [29][30]

$$T_I^{JLL'}(s^{\frac{1}{2}}, m_\Delta) \propto p^{L'} \frac{\omega_o \Gamma_o \left(\frac{q}{q_o}\right)}{\left(\omega^2 - \omega_o^2 + i\omega_o \Gamma_o \left(\frac{q}{q_o}\right)^3\right)}$$

where p is the momentum of the Δ in the centre-of-mass and q is the momentum of the final π and N in the Δ rest-frame.

The numerical factors are

$$\omega_o = 1236 \text{ MeV}$$

$$\Gamma_o = 120 \text{ MeV}$$

$$q_o = 225 \text{ MeV/c.}$$

Only the proportionality sign was kept and kinematic factors depending only on s were not retained since we made one-energy fits and normalisation was taken from experiment.

The angular dependence is in the term

$f^{JLL'}_{MM_S}(\Theta, \Phi, \phi_1, \theta^*)$ where Θ and Φ are defined above. In this section the x-axis is arbitrary except that it must be in the final-state plane. Other angles occurring are :

ϕ_1 = azimuthal angle of Δ in centre-of-mass

θ^* = angle of the pion in the Δ rest-frame defined as $\theta^* = 0$ with the two pions travelling in opposite directions in this frame.

These variables depend on $M^2_{\pi n'}$, $M^2_{\pi\pi'}$, $\ominus$ and Φ.

Suppressing some coefficients,

$$f^{JLL'}_{MM_S} = \sum_{M_L M'_S m} C^{L\ \frac{1}{2}\ J}_{M_L\ M\ (M_L+M)} C^{L'\ \ 3/2\ \ J}_{\left(\substack{M_L+M \\ -M'_S}\right)\ M'_S\ (M_L+M)}$$

$$\times\ C^{1\ \ \frac{1}{2}\ \ 3/2}_{M'_S-M_S\ \ M_S\ \ M'_S}$$

$$\times\ Y^{*}_{LM_L}(\ominus, \Phi)\ Y_{L'(M_L+M-M'_S)}(\pi/2, \phi_1)$$

$$\times\ Y_{1m}(\theta^{*}, 0)\, i^m\ d^1_{m(M'_S-M_S)}(\pi/2)$$

$$\times\ e^{i\phi_1(M'_S-M_S)}$$

In table V the explicit forms for M = 1/2 for various partial waves are given. The notation used in labelling the partial waves is LL' (2J) (2I); if I = 1/2, the last term is omitted. Waves permitted by angular momentum and parity selection rules are then

SD1, PP1, PP3, DS3, DD3, DD5, FP5

and higher waves, for I = 1/2 and I = 3/2.

From this angle-dependent formula, the following relations

are deduced :

(1) $L' + M_L + M - M'_S$ is even

(2) $M'_S = M_S \pm 1$

(3) $f^{JLL'}_{MM_S}(\Theta, \Phi, \phi_1, \theta^*) = (f^{JLL'}_{-M-M_S}(\Theta, \Phi, \phi_1, \theta^*))^* \times (-1)^{M-M_S}$

Further, waves differing in total angular momentum or parity do not interfere in the Dalitz Plot or its projections. Effective mass distributions depend strongly on the form of the angular dependence of the decay distribution. For instance, because of the $(1 + 3\cos^2\theta)$ decay angular distribution of the isobar the spin $-\frac{1}{2}$ waves give $\pi^+\pi^-$mass^2 spectra sharply peaked at both high and low ends. In fig. 15 the (mass)^2 spectra due to various Δ -production waves are shown for 552 MeV/c $\pi^+\pi^-$n.

IV.4 The Nσ Channel

A. The $\pi\pi$ s-wave phase shift δ_{00}

The $\pi\pi$ interaction, σ, is described in terms of the $I = J = 0$ $\pi\pi$ phase shift δ_{00}. There is, unfortunately, no reliable experimental information on $\pi\pi$ phase shifts below 500 MeV. Indeed, experimentally, $\pi\pi$ phase shifts can be measured only in situations with one or both π's off the mass-shell. The method of greatest success has been the study of

the reaction $\pi^- p \to \pi\pi N$ and $\pi\pi\Delta$, using Chew-Low extrapolations to isolate the one-pion-exchange contributions [31] [32]. This work has indicated that δ_{00} passes near 90° near 720 MeV total $\pi\pi$ energy. It is a matter of interest to determine the explicit dependence on energy, [32] [33] particularly near threshold where some theoretical calculations are available. However at low $\pi\pi$-masses there are so few data that no conclusions can be drawn [34]. The same defect holds in the theoretically cleaner study of K_{e4} decay [35]. Other methods such as the study of $K \to 3\pi$ [36], and $\eta \to 3\pi$ decay [37] and the rates for $K\pi 2$ decay [38], are of ambiguous interpretation.

Some direction provided by theoretical arguments was followed. The work of Morgan and Shaw [39] is of particular interest as it relates the $\pi\pi$ phase shifts below 500 MeV to the width of the resonance at 720 MeV. Two extreme cases are distinguished, viz. a resonance width of about 200 MeV gives δ_{00} small ($< 15^\circ$) up to 500 MeV and a width about 800 MeV gives δ_{00} rising smoothly from threshold up to 50° at 500 MeV. The results of a recent calculation by Lovelace using an amplitude of the Veneziano type gives $\pi\pi$ phase shifts of this second form (with scattering length $a_{00} = 0.29\ M_\pi^{-1}$) [40] [41].

Two forms of δ_{00} were used as $\pi\pi$ final state interaction factors in this work. First, a form having zero-scattering length, increasing approximately as q^3 from threshold (called here the C (cube) form) and secondly the Veneziano-Lovelace (V) form of δ_{00}. Both are referred to as a σ-state without

implying a low mass I = J = 0 resonance. Figure 16 shows the energy dependence of the two forms used. ρ-meson production (I = J = 1 $\pi\pi$ pair) was not considered. At the $\pi\pi$ masses accessible in this experiment, ($\lesssim 450$ MeV/c^2) , it is now believed [39] [40] that the p-wave phase shifts are small (below 5° at 500 MeV). A second, post facto, justification in ignoring ρ-production is that one can fit the $\pi^-\pi^0 p$ data, to which the σ does not contribute, with $\pi\Delta$ production alone (see section V).

The Watson final-state interaction [30] factor in the production matrix element was used. That is,

$$T \alpha p^{L'} q^{-1} (\cot \delta_{00} - i)^{-1}$$

where L' is the relative angular momentum of σ and N, p is their relative momentum and q is the π momentum in the dipion rest-frame.

B. Isobar formalism for Nσ

In a manner similar to that for the $\pi\Delta$ process (section IV.3), we write the production amplitude for the

$$\pi N \rightarrow \sigma N \qquad \sigma \rightarrow \pi\pi$$

mechanism.

$$T^{JLL'}_{MM_S}(\sigma N) = T^{JLL'}(s^{\frac{1}{2}}, m_\sigma)\, f^{JLL'}_{MM_S}(\Theta, \Phi)$$

$$f^{JLL'}_{MM_S}(\Theta, \Phi) = \sum_{M_L} C^{L\ \frac{1}{2}\ J}_{M_L\ M\ M_J} Y^*_{L\ M_L}(\Theta, \Phi)$$

$$Y_{L'M'_L}(\pi/2, \pi)\ \frac{1}{\sqrt{4\pi}}\ C^{L'\ \frac{1}{2}\ J}_{M'_L\ M_S\ M_J}$$

with $M'_L = M_J - M_S$

$M_J = M + M_L$.

The x-axis in this equation is along the neutron direction.

Table VI gives explicit forms for the allowed partial wave amplitudes, only from states of I = 1/2,

SP1, PS1, PD3, DP3, DF5, FD5.

V. Determination of Partial Wave Amplitudes

V.1 Fitting procedure

Distributions in eight variables, the three effective mass squared combinations, $\cos\Theta$, Φ and three production angles, were fitted. Theoretical distributions in these variables were obtained, using Monte Carlo techniques, for particular values of the complex amplitudes multiplying the factors discussed above, for the following set of partial waves :

$\pi\Delta$: SD1, PP1, PP3, DS3 and DS33 [42]

σN : SP1, PS1.

Best-fit values of the amplitudes and phases were obtained by minimizing

$$\chi^2 = \sum \left[\frac{N_{(exp)} - N_{(theory)}}{\Delta N_{(theory)}} \right]^2$$

with the sum taken over all bins of the eight histograms. The theoretical distributions were normalized to the total number of events so that absolute cross sections were not included as data to be fitted.

In making simultaneous fits to the $\pi^+\pi^-n$ and $\pi^-\pi^op$ distributions at 552 MeV/c, the number of $\pi^-\pi^op$ events was arbitrarily increased by a factor 4 to give the two sets of data approximately equal statistical weight [43].

V.2 Results of fit with $\pi\Delta$ Channel only

Both $\pi\Delta$ and σN channels were shown to be necessary because of the poor fits with predictions of the isobar model without the σ intermediate state. A fit with only $\pi\Delta$ channel amplitudes was unsuccessful in two important respects. The high mass $\pi^+\pi^-$ enhancement in the $\pi^+\pi^-n$ final state was not reproduced. No combination of partial waves yielded a high-mass peaking without at the same time requiring a low-mass peak (see figure 15 and the remarks at the close of section IV.3). The absence of interference, in the mass spectra, between waves of different J or P enables one to make this statement with confidence. Further, the branching ratio $\sigma(\pi^+\pi^-n)/\sigma(\pi^-\pi^op)$ at 552 MeV/c is not given correctly. The

experimental ratio is significantly larger than that obtainable from any partial wave, as shown in Table VII. No mixture of waves can produce the observed cross sections' ratio.

It is clear that some mechanism other than $\pi\Delta$ production contributes substantially to the $\pi^+\pi^-n$ state and causes the distribution in the $\pi^+\pi^-$ effective mass spectrum. Satisfactory fits were obtained to the $\pi^-p\pi^o$ data however with the $\pi\Delta$ mechanism alone. Thus it is indicated that there is no significant effect due to I = 1, J = 1 ρ-meson production so that the significant $\pi\pi$ final state interaction is likely in the I = 0 state.

V.3 Results of fit with $\pi\Delta$ and σN Channels

A sequence of fits to the data with the predictions of the isobar model following the procedure outlined above was made with both the C and V forms of $\pi\pi$ phase shifts. This included :

1. a fit to both final states at 552 MeV/c.
2. using the results of these fits as starting values, a fit to each data set individually.

This procedure should find in case (2) a solution similar to that in case (1), if it exists. Questions of uniqueness have been evaded.

In Figures 8 to 15 the theoretical predictions using best-fit parameters are shown superimposed on the experimental

histograms and in table VIII the partial wave amplitudes and χ^2 per degree of freedom of the fits are given.

The normalisation is to one event in $\pi^+\pi^-n$ at each energy (i.e. $a_{P3} = 1$ if the reaction proceeds entirely through PP3 etc.).

The parameters obtained in the fits are :

a_{P3} = PP3 amplitude

a_{D3} = sum of DS3 and DS33 amplitudes

p_{D13} = DS3/(DS3 + DS33)

a_{S1} = (SD1 + SP1) amplitude

p_{SD1} = SD1/(SD1 + SP1)

a_{P1} = (PP1 + PS1) amplitude

p_{PP1} = PP1/(PP1 + PS1)

together with the phases of the various waves. These variables were chosen as they are substantially uncorrelated, so that a simple calculation of the errors suffices [44]. Since the phases show very little energy dependence, we do not quote them in the table.

The notation used is C and V for simultaneous fits to $\pi^+\pi^-n$ and $\pi^-\pi^0p$ at 552 MeV/c, and C55, C50, C45, $C\pi^0$ for fits to one data set only.

Examination of the graphs and χ^2 per degree of freedom shows that whilst all the principal features of the data are accounted for by the model, there are some residual discrepancies,

particularly in the angular distributions. The sharp high π^-n mass peak in the theory, but not in the data, is probably due to the neglect of the spread in beam momentum in the Monte-Carlo calculation.

In all cases the C fits are better, having smaller χ^2 per degree of freedom, than the V fits. On these grounds one prefers variation of δ_{00} with $\pi\pi$ mass below 500 MeV which is more consistent with a 'narrow' resonance (about 200 MeV wide), or with a small scattering length than with a broad one. However, this statement must be taken with some caution. Since the best fit is not a good fit, it is conceivable that a V-type solution with some extra terms might prove superior. The fits to $\pi^-\pi^0p$ alone have good χ^2 per degree of freedom, justifying the neglect of ρ-production.

VI. Partial Wave Inelasticities

Using the fitted amplitudes of section V.2 and the cross-sections of section II.2 one can predict the values of $\sqrt{1-\eta^2}$ for the various πN partial waves. All the inelasticity is via the $\pi\pi N$ channel [45] and predictions can be made for the unobserved final states ($\pi^0\pi^0n$, $\pi^+\pi^+n$, $\pi^+\pi^0p$) using the isobar model.

The inelastic scattering total cross section is given by :

$$\sigma_{inel.} = \frac{\pi}{k^2} \sum_{\ell,J} (J + \tfrac{1}{2}) (1 - \eta^2_{\ell J})$$

where $k = \hbar/p$, p is the centre-of-mass momentum, and η is

the inelasticity parameter.

Table IX gives the values of $\sqrt{1 - \eta_{\ell J}^2}$ for the various partial waves, together with the 530 MeV/c results of the Saclay group [46] for comparison. Figures 17 and 18 show the energy dependence of $\sqrt{1 - \eta_{\ell J}^2}$ from this analysis and from the CERN [8] experimental and theoretical and the Glasgow [47] A and B analyses. These results show that inelasticity is not well determined by the elastic phase shift analyses. In those computational procedures η is sometimes either artificially smoothed to 1, unphysically greater than 1, or disconnected [4]. The agreement of the predictions of this work with the (independent) work at Saclay is good. The eleastic scattering data do not prefer one set of values of $\eta_{\ell J}$ over another, and so are not useful in determining the energy dependence of δ_{00}.

VII. The P_{11} branching ratio

Assuming that πN, $\pi\Delta$, and σN are the only open channels, total amplitudes for decay of the P_{11} intermediate state can be determined from these fits to the model. Since the inelastic processes are coherent, individual rates for the $\pi\Delta$ and σN decays cannot be inferred. The relative magnitudes of the various decay amplitudes provide a measure of the coupling of the P_{11} isobar to the $\pi\Delta$ and σN even though the interpretation as decay branching ratios is tenuous at best. Further, even ignoring the interference term in the decay intensity there is still uncertainty in the interpretation of the relative magnitudes of the $\pi\Delta$ and σN amplitudes, since the maximum center-of-mass energy in this work does not reach the resonance maximum. Also, no attempt has been made to separate resonance from possible background amplitudes.

Using the fitted PP1 and PS1 amplitudes, ignoring the interference

between $\pi\Delta$ and σN, together with the CERN theoretical values of the πN elastic scattering phase shift δ_{11}, one obtains the branching ratios given in Table X. The "cross" terms in the square of the sum of amplitudes is approximately 20% of the diagonal terms for the "V" solutions, and consistent with zero for the "C" solutions. The relative couplings to $\pi\Delta$ and σN deduced from the fits depend strongly on the character of the object called "σ". In the C solutions, the $\pi\Delta$ coupling is very small, whereas in the V solution the $\pi\Delta$ mode is comparable in strength with σN, becoming relatively more important as the energy increases.

VIII. Summary of Conclusions

The "Kirz-anomaly" [1], that is the high-mass peak in the $\pi^+\pi^-$ spectrum in $\pi^-p \to \pi^+\pi^-n$, has been explained over a range of incident π^- momenta by the introduction of an I = J = 0 $\pi\pi$ interaction. All the features of $\pi^-p \to \pi^-p\pi^0$ have been fitted without any I = J = 1 $\pi\pi$ interaction. There is a discrepancy of marginal statistical significance between theory and experiment in the shape of the $\pi^-\pi^0$ mass^2 spectrum, the experimental spectrum being more sharply peaked. The data of the Saclay group [46] at 530 MeV/c show the same effect.

Two types of energy dependence of δ_{00} have been considered (figure 16). In the Veneziano-Lovelace form [40] δ_{00} rises approximately linearly from threshold, passing through 90° near 720 MeV: the other form has δ_{00} rising from threshold as q^3 for energies less than 450 MeV and would give a narrower resonance than the first form. It has not been necessary to invoke a resonance with peak in the mass-range investigated. The results favour the q^3 form as the χ^2 are consistently better.

However, some modifications retaining the basic Veneziano-type $\pi\pi$ interaction might give a better fit. The Veneziano fit, including the $\pi\Delta$ mechanism, is far better than that of Roberts and Wagner [48] to fewer data.

There is substantial Δ-production at incident momenta as low as 456 MeV/c (1339 MeV centre-of-mass) rather far below the threshold for production of a Δ of mass 1236 MeV.

With the results of the fit to "isobar" model predictions, we have calculated partial wave inelasticities in the S_{11}, P_{11}, P_{13}, D_{13}, D_{33} partial waves, as a function of energy.

These results are only qualitatively in agreement with those following from the CERN elastic phase shift analysis [8]. We find inelasticity in the S_{11}, P_{13}, and D_{13} waves at lower energies than that analysis. The increasing inelasticities obtained here are consistent with the interpretation that P_{11} and D_{13} waves resonate at energies higher than those available in the present experiment.

The results of our analysis, and that of the Saclay group [46] from 530 to 760 MeV/c are compatible.

We have derived values of the P_{11} branching ratios into πN, $\pi\Delta$, and σN where σ is an $I = J = 0$ interacting $\pi\pi$ pair. The πN branching ratio is between 43% at 1339 MeV and 60% at 1402 MeV. The branching ratio between $\pi\Delta$ and σN depends, not surprisingly, on the form of σ used. In the preferred form the inelasticity is almost entirely through σN: with the Veneziano-Lovelace form of δ_{00} the ratio of $\pi\Delta$ to σN couplings is about unity and increases with energy.

REFERENCES AND FOOTNOTES

[1] J. Kirz, J. Schwartz and R.D. Tripp, Phys.Rev. 130 2481 (1963).

[2] C.N. Vittitoe, B.R. Riley, W.J. Fickinger, V.P. Kenney, J.G. Mowat and W.D. Shephard, Phys.Rev. 135B 232 (1964).

S. Femino, S. Janelli and F. Mezzanares, Nuovo Cimento 52A 892 (1967).

L. Bertanza, A. Bigi, R. Carrara, R. Casali, Nuovo Cimento 44A 712 (1966).

R.A. Burnstein, G.R. Charlton, T.B. Day, G. Quareni, A. Quareni-Vignudelli, G.B. Yodh and I. Nadelhaft, Phys.Rev. 138B 1044 (1965).

J.D. Oliver, I. Nadelhaft and G.B. Yodh, Phys.Rev. 147 932 (1966).

M. Banner, J.F. Deteouf, M.L. Fayoux, J.L. Hamel, J. Zsembery, J. Cheze and J. Teiger, Phys.Rev. 166 1346 (1968).

[3] R. Sternheimer and S. Lindenbaum, Phys.Rev. 109 1723 (1958).

[4] R. Plano. Rapporteur's talk at the Lund International Conference on Strong Interactions (1969). (To be published.)

[5] $\pi^-p/\pi^-p\pi^o$ ambiguities arise chiefly in backwards elastic scatters, the number of which is not large. The effect of the scanning loss of short-proton events on the $\pi^-\pi^o$ mass spectrum has been calculated and shown to be spread over a range of masses and always less than the statistical error. (The loss is typically $3 \pm 1\%$ in the mass range 280 to 300 MeV/c^2.)

[6] D.H. Saxon. D.Phil. Thesis HGP/T/6 (Rutherford High Energy Laboratory, Chilton, Berks, England 1970).

[7] Within the errors they are consistent with interpolations of the CERN "theoretical" phase shifts; see reference [8].

[8] A. Donnachie, R.G. Kirsopp and C. Lovelace. CERN/TH 838 addendum.

[9] P.M. Ogden, D.E. Hagge, J.E. Helland, M. Banner, J-F Deteouf, J. Teiger, Phys.Rev. 137B 1115 (1965).

[10] G.B. Yodh, Univ. of Maryland Tech. report 512 (1965).

[11] S.M. Berman and M. Jacob, Phys.Rev. 139B 1023 (1965).

[12] D. Branson, P.V. Landshoff and J.C. Taylor, Phys.Rev. 132 902 (1963).

[13] R.C. Arnold and J.L. Uretsky, Phys.Rev. 153 1443 (1967).

[14] D. Morgan, Phys.Rev. 166 1731 (1968).

[15] B. Deler and G. Valladas, Nuovo Cimento 45A 559 (1966).

[16] M.G. Bowler and R.J. Cashmore (submitted to Nuclear Physics B).

[17] It is not possible to determine the parity of a particular wave without polarization information or the use of a dynamical model. This point has sometimes been neglected.

[18] L.D. Faddeev, Zhur. Eksp. i. Teoret. Fiz. 39 1459 (1960).

L.D. Faddeev, AERE Translation 1002 (Harwell 1964).

[19] M. Froissart and R. Omnes, Physique des Hautes Energies - les Houches 1965, p. 177 ff. (Gordon and Breach).

[20] C. Lovelace, Phys.Rev. 135B 1225 (1964).

[21] D.Z. Freedman, C. Lovelace and J.M. Namyslowski, Nuovo Cimento 53 258 (1966).

[22] I.J.R. Aitchison, Nuovo Cimento 51A 249, 272 (1967).
I.J.R. Aitchison, Phys.Rev. 133B 1257 (1964).

[23] V.V. Anisovich and L.G. Dakhno, Phys.Lett. 10, 221 (1964).

[24] V.V. Anisovich, E.M. Levin, A.K. Likhoded, Y.G. Stroganov, Sov. J.N.P. 8 339 (1969).

[25] Batusov et al. JETP 16 1422 (1963).

[26] J.M. Namyslowski, M.S.K. Razmi and R.G. Roberts, ICTP/65/20 (Imperial College, London) and Phys.Rev. 157 1328 (1967).

[27] G. Wick, Ann. Phys. (NY) 18 65 (1962).

[28] This base is not Lorentz Invariant. However, Stapp (Phys.Rev. 103 425 (1956)) has shown that the most important relativistic effect is a rotation of the polarization of the isobar when a Lorentz transformation is made from the centre-of-mass for production to the centre-of-mass for decay. This angle is typically less than 3^{o} at these energies. One therefore neglects the effect.

[29] K.M. Watson, Phys. Rev. 85 852 (1952).

[30] J.D. Jackson, CERN/TH 416 (1964).

[31] J.P. Baton, G. Laurens and J. Reignier, Nucl.Phys. B3 349 (1967).

[32] L.J. Gutay, D.D. Carmony, P.L. Csonka, F.J. Loeffler and F.T. Meiere, Purdue University report COO-1428-65 (unpublished).

G.L. Kane and M. Ross, Phys.Rev. 177 2353 (1969).

P.B. Johnson, J.A. Poirier, N.N. Biswas, N.M. Cason, T.H. Groves, V.P. Kenney, J.T. McGahan, W.D. Shephard, L.J. Gutay, J.H. Campbell, R.L. Elsner, F.J. Loeffler, R.E. Peters, R.J. Sahni, W.L. Yen, L. Derado, Z.G.T. Guragossian, Phys.Rev. 176 1651 (1968).

L.J. Gutay, Proc. Argonne Conference on $\pi\pi$ and $K\pi$ Interactions (1969), p. 241 ff.

W.D. Walker, J. Carroll, A. Garfinkel and B.Y. Oh, Phys.Rev. Lett. 18 630 (1967).

E. Colton and P.E. Schlein, Proc. Argonne Conf. p.1 ff.

E. Malamud and P.E. Schlein, Proc. Argonne Conf. p. 93 ff.

[33] G.A. Smith and R.J. Manning, Phys.Rev. 171 1399 (1968).

I.F. Corbett, C.J.S. Damerell, N. Middlemas, D. Newton, A.B. Clegg, W.S.C. Williams and A.S. Carroll, Phys. Rev. 156 1451 (1967).

[34] N.N. Biswas, N.M. Cason, P.B. Johnson, V.P. Kenney, J.A. Poirier, W.D. Shephard and R. Torgerson, Phys.Lett. 27B 513 (1968).

[35] F.A. Berends, A. Donnachie and G.C. Oades, Nucl. Phys. B3 569 (1967).

R.P. Ely, G. Gidal, V. Hagopian, G.E. Kalmus, K. Billing, F.W. Bullock, M.J. Esten, M. Govan, C. Henderson, W.L. Knight, F.R. Stannard, O. Treutler, U. Camerini, D. Cline, W.F. Fry, H. Haggerty, R.H. March and W.J. Singleton, Phys.Rev. 180 1319 (1969).

A. Pais and S.B. Treiman, Phys.Rev. 168 1858 (1968).

N. Cabibbo and A. Maksymowicz, Phys.Rev. 137B 438 (1965).

[36] D. Davison, R. Bacastow, W.H. Barkas, D.A. Evans, S-Y Fong, L.E. Porter, R.T. Poe and D. Greiner, Phys.Rev. 180 1333 (1969).

R.N. Chaudhuri, Phys.Rev. 175 2066 (1968).

L.M. Brown and P. Singer, Phys.Rev. 133B 812 (1964).

A.N. Mitra and S. Ray, Phys.Rev. 135B 146 (1964).

N.N. Khuri and S.B. Treiman, Phys.Rev. 119 1115 (1960).

G. Gribov, JETP 14 871 (1962).

A. Anisovich, JETP 17 1072 (1963).

A. Anisovich, JETP 20 161 (1965).

M. Baldo-Coelin et al. N.C. 6 84 (1957).

S. McKenna et al. N.C. 10 763 (1958).

G. Kalmus et al. Phys.Rev. Lett. 13 99 (1964).

[37] A. Laribbe, A. Leveque, A. Muller, E. Pauli, D. Revel, B. Tallini, P. Litchfield, L.K. Rangan, A.M. Segar, J.R. Smith, P.J. Finney, C.M. Fisher and E. Pickup, RPP/H/17.

F.S. Crawford, R.A. Grossman, L.J. Lloyd, L.R. Price and E.C. Fowler, Phys.Rev.Lett. 11, 564 (1963).

[38] T.D. Lee and C.S. Wu, Ann.Rev.Nuc.Sci. 16 528 (1966).

[39] D. Morgan and G. Shaw, Nuclear Physics B10 261 (1969).

[40] C. Lovelace, Proceedings of Argonne Conference on $\pi\pi$ and $K\pi$ Interactions (1969) p. 562 and CERN/TH 1041 (1969).

[41] F. Wagner, CERN/TH 1012 (1969).

[42] This I = 3/2 wave was included since the work of Bowler and Cashmore on π^+p inelastic reactions at 600 - 800 MeV/c [16] indicates that this is the dominant I = 3/2 $\pi N \rightarrow \pi\Delta$ wave and that all others are small. In I = 1/2 $\pi\Delta$ production in $\pi^-p\pi^o$, the $\Delta^+\pi^-$ and $\Delta^o\pi^o$ amplitudes are equal and opposite, so that distributions should be invariant under an interchange of π^- and π^o, whereas experimentally there are significant differences in M^2 (πp) and cos $\bar{\theta}_\pi$ distributions. (See Figures 9 and 10).

[43] This is not a true χ^2 as we have taken eight projections of a four-dimensional space. (We make only one-energy fits.) However, there is clearly more information in a four dimensional space than in four orthogonal projections of it, so that no serious redundancy is introduced by attempting to fit all the distributions.

[44] The error on a parameter is defined as the change in that parameter from its value when χ^2 has its minimum which makes an increase in χ^2 to a value having a confidence level one-third that of the best fit. (There is then some ambiguity in the fits to both states

simultaneously as the function minimised is not a pure χ^2.) There are two ways of estimating this change. One can hold all other parameters constant at their best values or can change this parameter to a different value and reminimise χ^2 as a function of all the other parameters. The second scheme is more closely related to the experimental knowledge of the parameter. In this case the two methods agree to within 15% of their estimates of the errors, indicating that the parameters used are not severely correlated. The errors quoted are calculated by the first method.

[45] S.U. Chung et al. Phys.Rev. 165 1491 (1968).

[46] M. de Beer, B. Deler, J. Dolbeau, M. Neveu, Nguyen Thuc Diem, G. Smadja and G. Valladas (Submitted to Nuclear Physics B).

[47] A.T. Davies. Analysis of Nucleon Resonances below 2 GeV. Glasgow preprint (1969).

[48] R.G. Roberts and F. Wagner, CERN/TH 1014 (1969).

FIGURE CAPTIONS

Fig. 1. Elastic centre of mass scattering angular distribution at 499 MeV/c incident π^- momentum.

Fig. 2. Elastic centre of mass scattering angle distribution at 552 MeV/c incident π^- momentum.

Fig. 3. Dalitz plot for $\pi^- p \to \pi^+ \pi^- n$ at 456 MeV/c.

Fig. 4. Dalitz plot for $\pi^- p \to \pi^+ \pi^- n$ at 505 MeV/c.

Fig. 5. Dalitz plot for $\pi^- p \to \pi^+ \pi^- n$ at 552 MeV/c.

Fig. 6. Dalitz plot for $\pi^- p \to \pi^- \pi^0 p$ at 552 MeV/c.

Fig. 7. Mass^2 spectra at 552 MeV/c. Fitted distributions obtained with the "cube" form of $\pi\pi$ phase shift are superimposed on the experimental histograms.

Fig. 8. Mass^2 spectra at 552 MeV/c. Fitted distributions obtained with the "Veneziano" form of $\pi\pi$ phase shifts are superimposed on the experimental histograms.

Fig. 9. Angular distributions at 552 MeV/c with "cube" fits.

Fig. 10. Angular distributions at 552 MeV/c with "Veneziano" fits.

Fig. 11. Angular distributions and mass^2 spectra for $\pi^- p \to \pi^+ \pi^- n$ at 505 MeV/c with "cube" and Veneziano" fits.

Fig. 12. Angular distributions and mass^2 spectra for $\pi^- p \to \pi^+ \pi^- n$ at 456 MeV/c with "cube" and "Veneziano" fits.

Fig. 13. Expansion of a $2 \to 3$ body amplitude into isobar terms and triangle graphs.

Fig. 14. Mass^2 spectra from $\pi\Delta$ production in pure angular momentum waves for $\pi^+ \pi^- n$ at 552 MeV/c.

Fig. 15. Mass dependence of $\pi\pi$ scattering phase shift δ_{00} for the "cube" and "Veneziano" forms.

Fig. 16. Incident momentum dependence of the inelasticity $\sqrt{1 - \eta^2}$ for S_{11}, P_{13}, and P_{33} partial waves inferred from this work and the elastic phase-shift analyses of references [8] and [47].

Fig. 17. Incident-momentum dependence of the inelasticity $\sqrt{1 - \eta^2}$ for D_{13} and D_{33} partial waves inferred from this work and the elastic phase-shift analyses of references [8] and [47].

Table I

Momentum (MeV/c)		Number of events after cuts		
Central Value	Limits accepted	$\pi^- p$	$\pi^+ \pi^- n$	$\pi^- p \pi^o$
552	536 - 566	6503	2241	528
505	490 - 520		1965	
499*	482 - 516	1386	298	47
456*	440 - 470		2591	

* Film taken with a 1/8" lead sheet at a double focus of the beam to reduce electron contamination.

Table II

Total Cross-sections (mb)

Momentum (MeV/c)	$\pi^+\pi^-n$	$\pi^-\pi^o p$
456	1.0 ± 0.2	0.17 ± 0.05
499	2.40 ± 0.16	0.32 ± 0.05
552	3.84 ± 0.16	0.87 ± 0.05

Table III

W_{KM} moments, integrated over the Dalitz Plot for $\pi^+\pi^-n$

K	M	456 MeV/c	505 MeV/c
1	1	$-.066\pm.008 + i(-.066\pm.008)$	$-.055\pm.009 + i(-.079\pm.009)$
2	0	$.020 \pm .012$	$.023 \pm .010$
2	2	$.0062\pm.0061 + i(.018\pm.006)$	$-.006\pm.006 + i(-.008\pm.006)$
3	1	$-.009 \pm .005 + i(-.003\pm.005)$	$.001\pm.006 + i(-.013 \pm .006)$
3	3	$.010\pm.005 + i(-.001\pm.005)$	$.004\pm.006 + i(-.008\pm.006)$
4	0	$-.014 \pm .007$	$-.019 \pm .008$
4	2	$-.007\pm.005 + i(-.005\pm.005)$	$-.002\pm.005 + i(.004 \pm .005)$
4	4	$-.002\pm.005 + i(.010\pm.005)$	$-.004\pm.005 + i(.004 \pm .005)$
5	1	$.003\pm.004 + i(-.003\pm.004)$	$.008\pm.005 + i(.007\pm.005)$
5	3	$.005\pm.004 + i(.003\pm.004)$	$.001\pm.005 + i(.001\pm.005)$
5	5	$.002\pm.004 + i(-.003\pm.004)$	$-.009\pm.005 + i(-.003\pm.005)$

Table III (continued)

W_{KM} moments, integrated over the Dalitz Plot at 552 MeV/c

K	M	$\pi^+\pi^-n$	$\pi^-\pi^0p$
1	1	$-.070\pm.009 + i(-.080\pm.008)$	$-.035\pm.019 + i(.038\pm.017)$
2	0	$-.001 \pm .009$	$-.019 \pm .019$
2	2	$.012\pm.007 + i(.031\pm.007)$	$.037\pm.014 + i(.015\pm.014)$
3	1	$-.014\pm.006 + i(-.003\pm.006)$	$.004\pm.011 + i(.001\pm.012)$
3	3	$.009\pm.005 + i(-.006\pm.006)$	$.005\pm.012 + i(.037\pm.012)$
4	0	$.009 \pm .007$	$-.013\pm .014$
4	2	$.004\pm.005 + i(.006\pm.005)$	$-.015\pm.011 + i(.002\pm.010)$
4	4	$.004\pm.005 + i(.011\pm.005)$	$.009\pm.010 + i(-.006\pm.010)$
5	1	$.007\pm.005 + i(.001\pm.005)$	$.004\pm.009 + i(.008\pm.009)$
5	3	$-.008\pm.004 + i(-.001\pm.005)$	$-.005\pm.010 + i(-.010\pm.009)$
5	5	$-.001\pm.005 + i(-.008\pm.005)$	$.010\pm.009 + i(.000\pm.009)$

Table IV

Confidence levels for the hypothesis that all W_{KMi} moments of a given K are zero within the statistics.

	K	1	2	3	4	5
$\pi^+\pi^-n$	456	$<.0001$	.006	.12	.08	.60
	505	$<.0001$	.04	.15	.15	.40
	552	$<.0001$	$<.0001$	.20	.10	.35
$\pi^-\pi^0p$	552	.015	.02	.03	.50	.75

Table V

Δ-production from M = ½. The arguments of the spherical harmonic are θ^*, ϕ_1 throughout.

WAVE	M_S	Amplitude
SD1	½	0
	-½	$-\frac{1}{2\sqrt{2}} Y^*_{00} e^{i\phi_1} (2\cos\theta^* - i\sin\theta^*)$
PP1	½	$\frac{1}{2\sqrt{6}} Y^*_{10} (2\cos\theta^* + i\sin\theta^*)$
	-½	$\frac{1}{2\sqrt{3}} Y^*_{1-1} (2\cos\theta^* - i\sin\theta^*)$
PP3	½	$\frac{1}{2\sqrt{30}} Y^*_{10} (\cos\theta^* + 5i\sin\theta^*)$
	-½	$\frac{1}{4\sqrt{15}} \left[3Y^*_{11} e^{2i\phi_1} (\cos\theta^* + i\sin\theta^*) + Y^*_{1-1} (5i\sin\theta^* - \cos\theta^*) \right]$
DS3	½	$\frac{1}{4}\sqrt{\frac{3}{5}} \left[Y^*_{21} e^{i\phi_1} [\cos\theta^* + i\sin\theta^*] + Y^*_{2-1} e^{-i\phi_1} [i\sin\theta^* - \cos\theta^*] \right]$
	-½	$\frac{1}{4}\sqrt{\frac{3}{5}} \left\{ \sqrt{\frac{2}{3}} Y^*_{20} e^{i\phi_1} [\cos\theta^* + i\sin\theta^*] + 2Y^*_{2-2} e^{-i\phi_1} [i\sin\theta^* - \cos\theta^*] \right\}$

Table V (continued)

WAVE	M_S	Amplitude
DD3	$\frac{1}{2}$	$\frac{1}{4}\sqrt{\frac{3}{5}}\left(-Y^*_{21}\cos\theta^* + Y^*_{2-1} e^{-i\phi_1}[2i\sin\theta^* + \cos\theta^*]\right)$
	$-\frac{1}{2}$	$\frac{1}{2}\left(\sqrt{\frac{1}{10}}\ Y^*_{20} e^{i\phi_1}[-\cos\theta^* + 2i\sin\theta^*] + \sqrt{\frac{3}{5}}\ Y^*_{2-2}\cos\theta^* e^{-i\phi_1}\right)$
DD5	$\frac{1}{2}$	$\frac{1}{2\sqrt{35}}\left(-Y^*_{21} e^{i\phi_1}[\cos\theta^* + 5i\sin\theta^*] + Y^*_{2-1} e^{-i\phi_1}[2i\sin\theta^* + \cos\theta^*]\right)$
	$-\frac{1}{2}$	$\frac{1}{4\sqrt{35}}\left(Y^*_{2-2} e^{-i\phi_1}[5i\sin\theta^* - \cos\theta^*] - 5Y^*_{22} e^{3i\phi_1}[\cos\theta^* + i\sin\theta^*] + \sqrt{6}\, Y^*_{20} e^{i\phi_1}[\cos\theta^* - 2i\sin\theta^*]\right)$
FP5	$\frac{1}{2}$	$\frac{1}{4}\sqrt{\frac{3}{7}}\left(Y^*_{32} e^{2i\phi_1}[\cos\theta^* + i\sin\theta^*] + Y^*_{3-2} e^{-2i\phi_1}[\cos\theta^* - i\sin\theta^*]\right) - \frac{3}{2}\frac{1}{\sqrt{70}}\ Y^*_{30}\cos\theta^*$
	$-\frac{1}{2}$	$\frac{1}{2}\sqrt{\frac{3}{70}}\left(Y^*_{31} e^{2i\phi_1}[i\sin\theta^* + \cos\theta^*] - 2Y^*_{3-1}\cos\theta^*\right) + \frac{3}{4}\sqrt{\frac{2}{7}}\ Y^*_{3-3} e^{-2i\phi_1}[\cos\theta^* - i\sin\theta^*]$

Table VI

σ-production from M = ½. The argument of the spherical harmonic are θ, φ throughout. x-axis along the outoing nucleon.

Wave	M_S	Amplitude
SP1	½	0
	-½	$\frac{1}{2} Y^*_{00}$
PS1	½	$-\frac{1}{2\sqrt{3}} Y^*_{10}$
	-½	$-\frac{1}{\sqrt{6}} Y^*_{1-1}$
PD3	½	$\frac{1}{2\sqrt{6}} Y^*_{10}$
	-½	$\frac{1}{4\sqrt{3}} (3Y^*_{11} - Y^*_{1-1})$
DP3	½	$\frac{1}{4}\sqrt{\frac{3}{5}} (Y^*_{2-1} - Y^*_{21})$
	-½	$\frac{1}{4}\sqrt{\frac{3}{5}} (2Y^*_{2-2} - \sqrt{\frac{2}{3}} Y^*_{20})$
DF5	½	$\frac{1}{4}\sqrt{\frac{2}{5}} (Y^*_{21} - Y^*_{2-1})$
	-½	$\frac{1}{8} \frac{1}{\sqrt{15}} (Y^*_{22} 5\sqrt{6} - 6Y^*_{20} + \sqrt{6} Y^*_{2-2})$

- continued -

Table VI (continued)

Wave	M_S	Amplitude
FD5	$\frac{1}{2}$	$-\frac{1}{4}\sqrt{\frac{5}{14}}\ (Y^*_{32} + Y^*_{3-2}) + \frac{\sqrt{3}}{4\sqrt{7}}\ Y^*_{30}$
	$-\frac{1}{2}$	$\frac{1}{4}\frac{1}{\sqrt{7}}(-Y^*_{31} + 2\ Y^*_{3-1} - \sqrt{15}\ Y^*_{3-3})$

Table VII

Predicted branching ratios $\sigma(\pi^+\pi^-n) / \sigma(\pi^-\pi^0 p)$ at 552 MeV/c.

Partial wave	Branching ratio
SD1	2.33
PP1	3.70
PP3	1.32
DS3	2.97
DS33	1.54
Experiment	4.22 ± 0.21

Table VIII

Fit	$\frac{\chi^2}{NDF}$	a_{P3}	a_{D3}	p_{D13}	a_{S1}	p_{SD1}	a_{F1}	p_{FP1}
C	2.4	.28 ±.09	.74 ±.13	.86 ±.17	.51 ±.21	.36 ±.16	.71 ±.12	.22 ±.21
C55	2.1	.27 ±.07	.72 ±.05	.58 ±.11	.62 ±.10	.28 ±.10	.76 ±.04	.32 ±.19
Cπ^o	1.2	.29 ±.08	.93 ±.29	.68 ±.09	.15 ±.11	1	.32 ±.19	1
V	2.5	.19 ±.10	.76 ±.09	.70 ±.09	.34 ±.20	.35 ±.36	1.00 ±.10	.50 ±.10
V55	2.8	.23 ±.07	.64 ±.04	.55 ±.12	.40 ±.08	.22 ±.15	1.01 ±.05	.48 ±.03
Vπ^o	1.4	.32 ±.05	.80 ±.12	.81 ±.08	.16 ±.11	1	.02 ±.01	1
C50	2.0	.38 ±.07	.57 ±.06	.53 ±.16	.47 ±.11	.21 ±.13	.78 ±.05	.25 ±.09
V50	2.6	.34 ±.06	.49 ±.06	.60 ±.16	.34 ±.09	.25 ±.20	1.03 ±.04	.46 ±.04
C45	1.7	.35 ±.06	.50 ±.06	.41 ±.14	.47 ±.10	.23 ±.10	.84 ±.04	.21 ±.07
V45	2.4	.21 ±.07	.40 ±.05	.58 ±.16	.30 ±.11	.39 ±.17	1.12 ±.04	.43 ±.03

Table IX

Values of $\sqrt{1 - \eta^2}$

	S_{11}	P_{11}	P_{13}	D_{13}	D_{33}
C45	.14 ± .03	.30 ± .03	.13 ± .03	.07 ± .01	.14 ± .03
C50	.24 ± .05	.43 ± .04	.23 ± .04	.18 ± .04	.21 ± .05
C55	.41 ± .07	.56 ± .05	.21 ± .06	.27 ± .05	.32 ± .05
C	.35 ± .13	.48 ± .11	.23 ± .09	.59 ± .11	.09 ± .09
V45	.09 ± .03	.32 ± .05	.08 ± .02	.08 ± .02	.08 ± .02
V50	.19 ± .05	.51 ± .02	.22 ± .03	.16 ± .04	.15 ± .03
V55	.31 ± .03	.68 ± .07	.19 ± .06	.30 ± .06	.31 ± .06
V	.24 ± .14	.63 ± .07	.13 ± .08	.39 ± .05	.21 ± .03
Saclay (530 MeV/c)	.17	.58	.08	.22	.36

Table X

P_{11} branching ratios calculated from the fits to the data.

	πN	$\pi \Delta$	σN
'C' solutions			
1340 MeV	.43 ± .05	.03 ± .05	.54 ± .05
1370 MeV	.60 ± .10	.04 ± .12	.36 ± .12
1400 MeV	.63 ± .07	.09 ± .10	.28 ± .10
1400 MeV (both states fitted)	.67 ± .18	.03 ± .20	.30 ± .20
'V' solutions			
1340 MeV	.42 ± .17	.22 ± .17	.36 ± .17
1370 MeV	.50 ± .16	.23 ± .16	.27 ± .16
1400 MeV	.54 ± .10	.23 ± .10	.23 ± .10
1400 MeV (both states fitted)	.58 ± .09	.22 ± .12	.20 ± .12

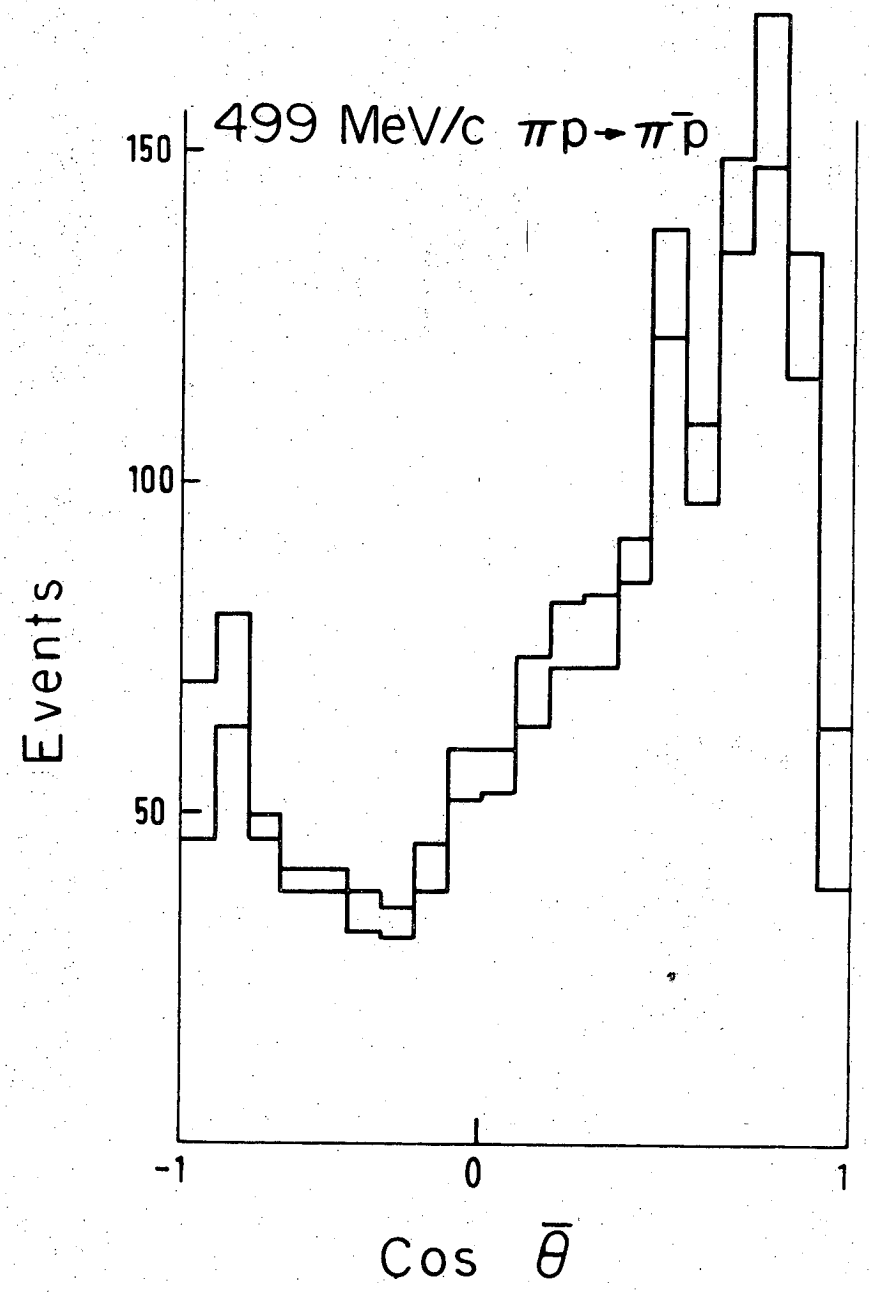

XBL703-2554

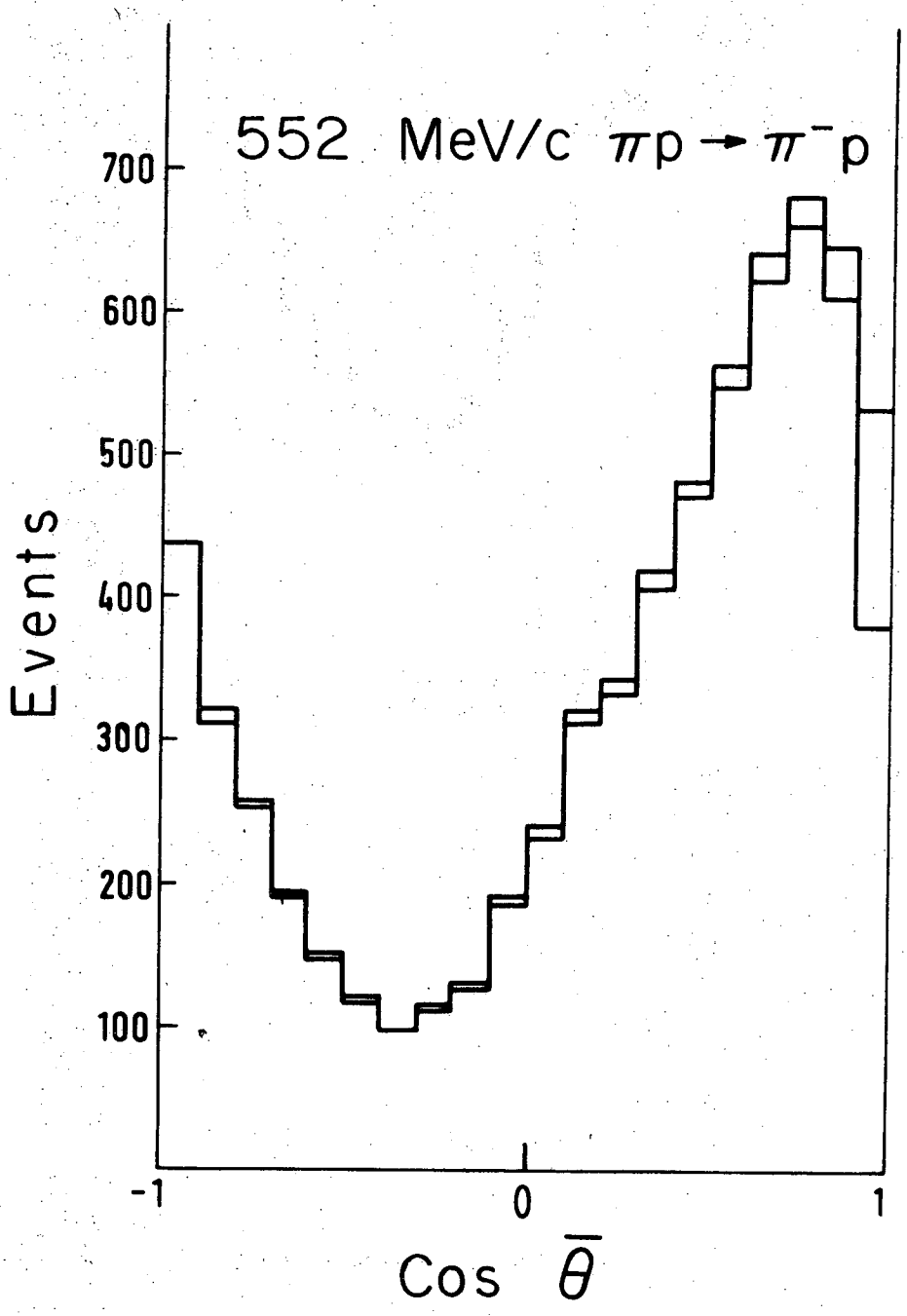
552 MeV/c $\pi p \rightarrow \pi^- p$
Events
700
600
500
400
300
200
100
-1
0
1
Cos $\bar{\theta}$

XBL703-2551

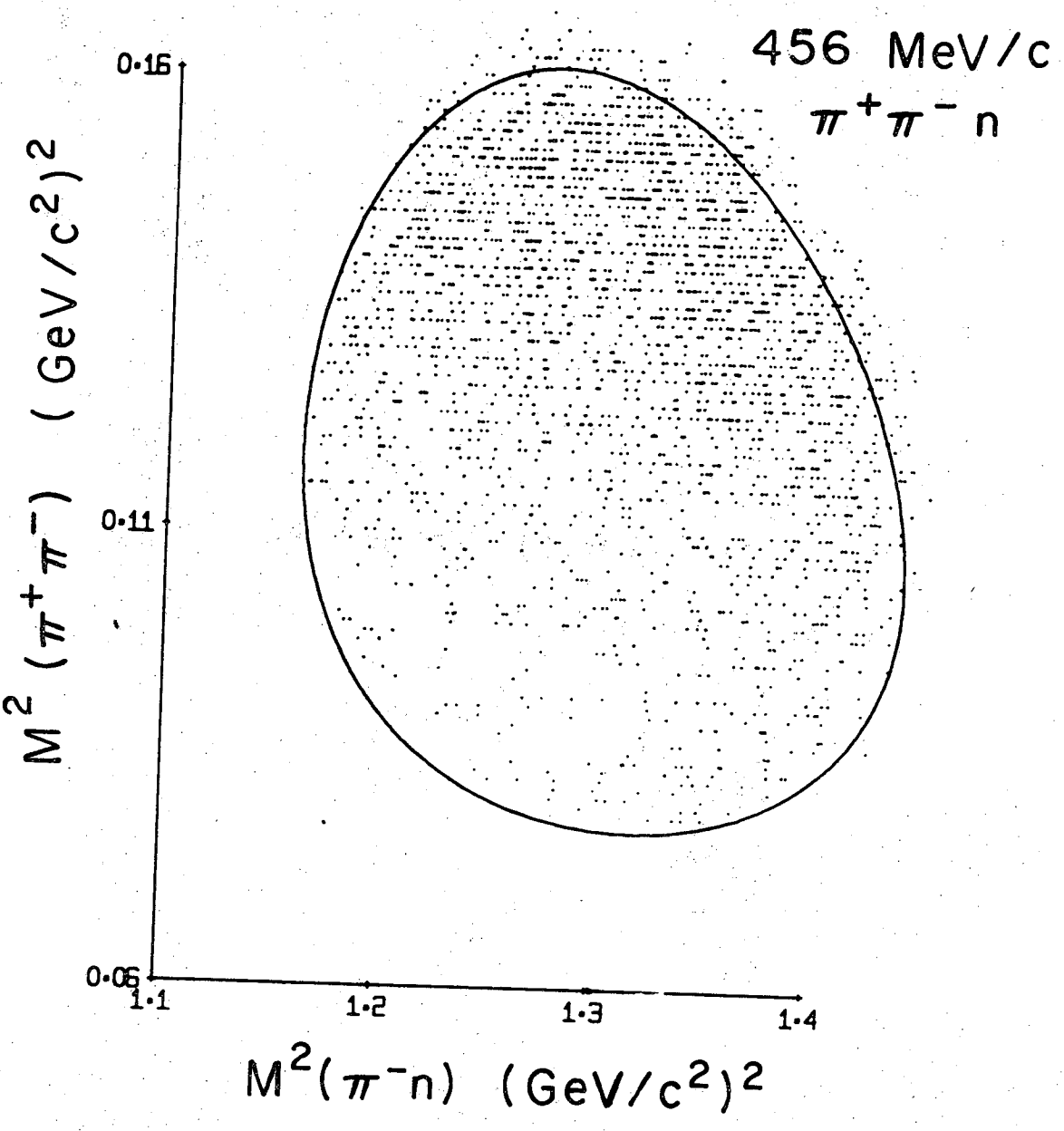
456 MeV/c
$\pi^+\pi^-$ n
0·15
0·11
0·06
$M^2(\pi^+\pi^-)$ (GeV/c^2)^2
1·1
1·2
1·3
1·4
$M^2(\pi^-n)$ (GeV/c^2)^2

XBL703-2555

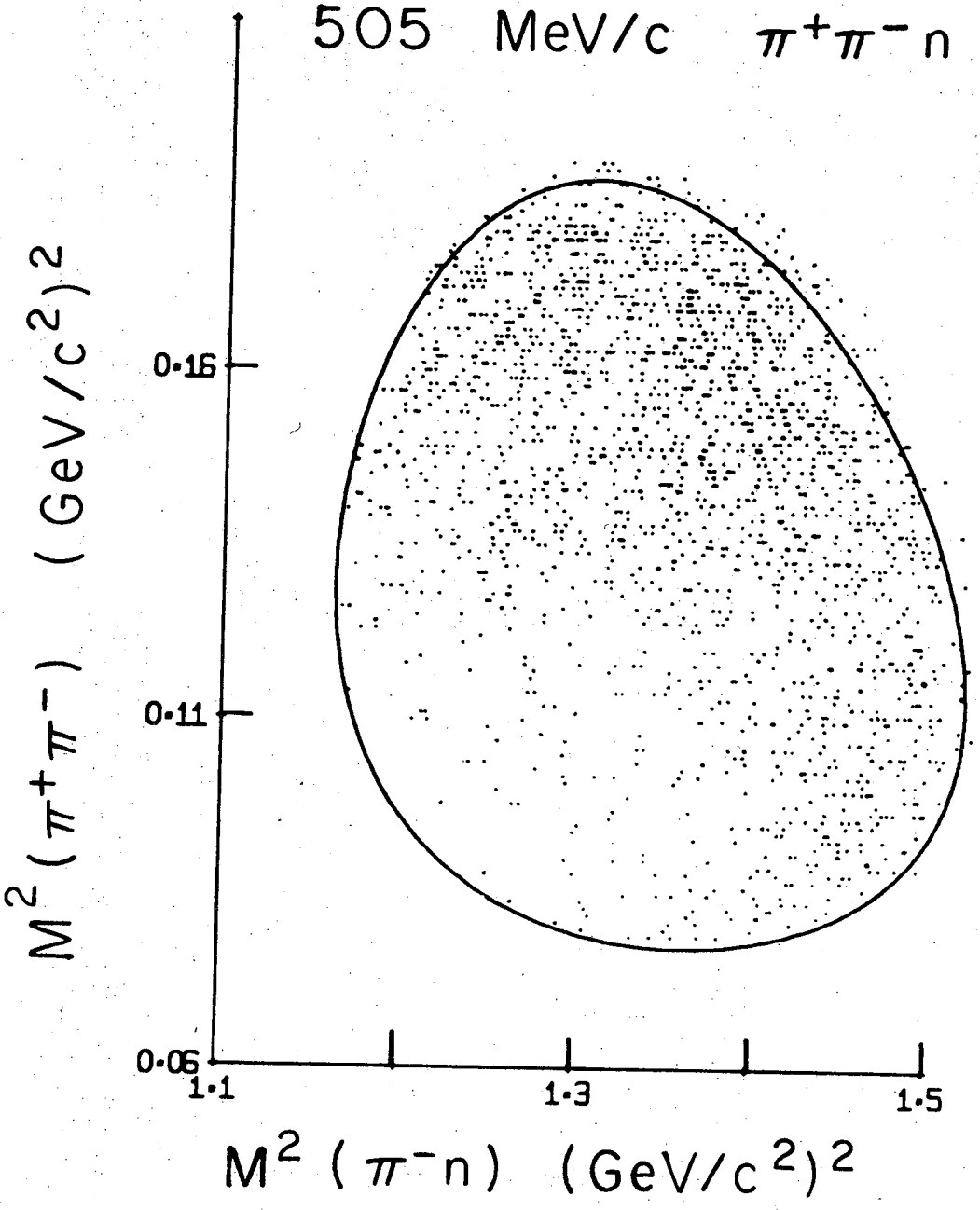
505 MeV/c $\pi^+\pi^-$ n
$M^2(\pi^+\pi^-)$ $(GeV/c^2)^2$
0.16
0.11
0.06
1.1
1.3
1.5
$M^2(\pi^-n)$ $(GeV/c^2)^2$

XBL703-2544

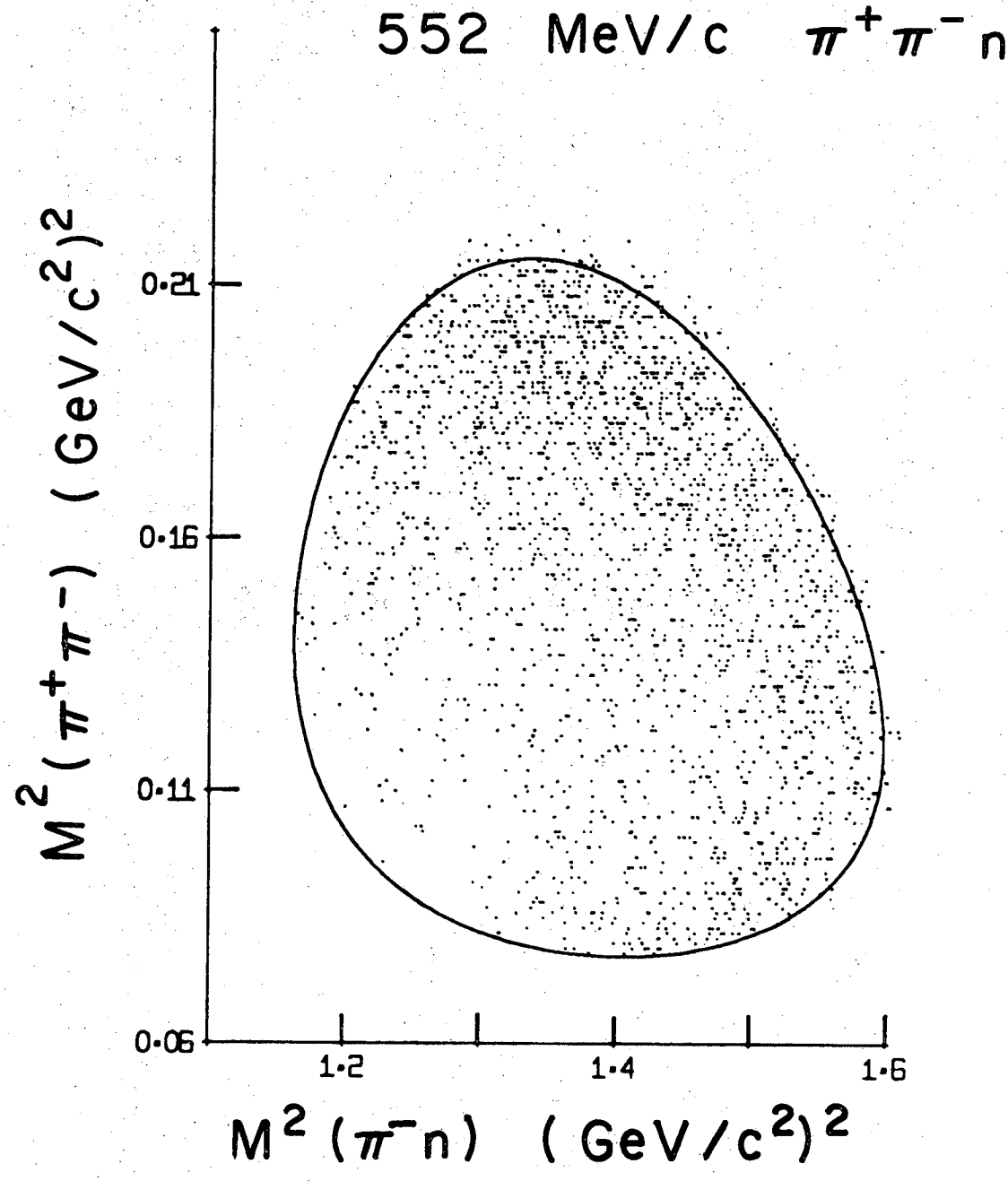
552 MeV/c $\pi^+\pi^-$ n
$M^2(\pi^+\pi^-)$ $(GeV/c^2)^2$
0·21
0·16
0·11
0·06
1·2
1·4
1·6
$M^2(\pi^-n)$ $(GeV/c^2)^2$

XBL703-2543

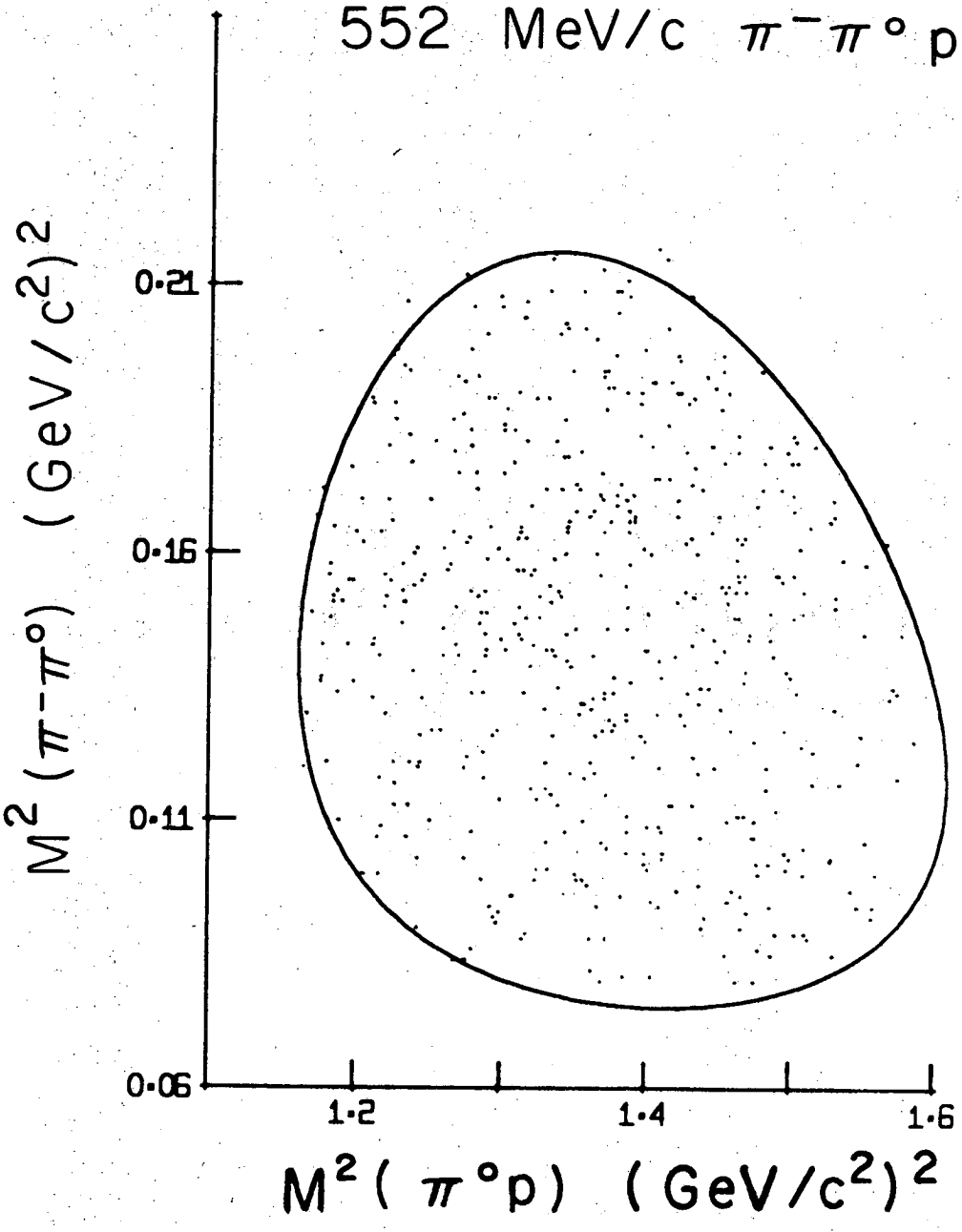
552 MeV/c $\pi^-\pi^\circ$ p
$M^2(\pi^-\pi^\circ)$ $(GeV/c^2)^2$
0·21
0·16
0·11
0·06
1·2
1·4
1·6
$M^2(\pi^\circ p)$ $(GeV/c^2)^2$

XBL703-2545

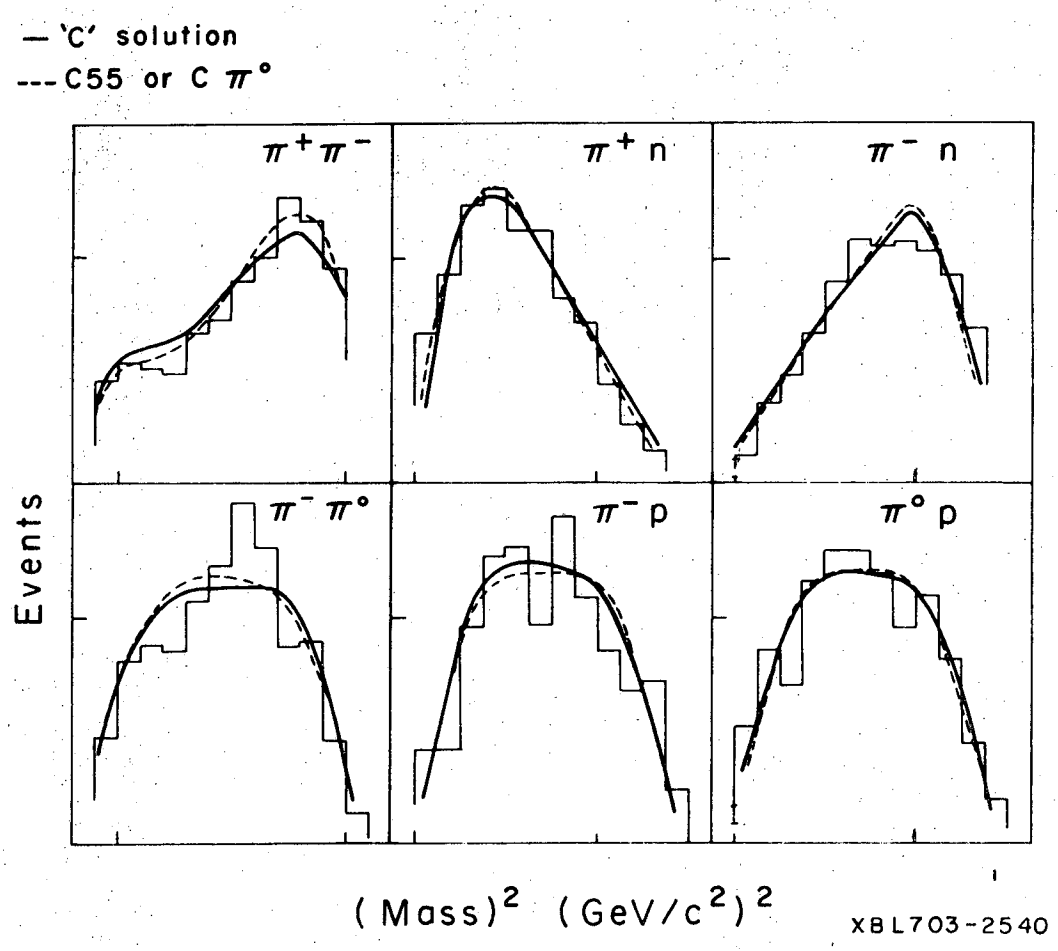
— 'C' solution
--- C55 or C π°
π⁺π⁻
π⁺ n
π⁻ n
π⁻ π°
π⁻ p
π° p
Events
(Mass)² (GeV/c²)²
XBL703-2540

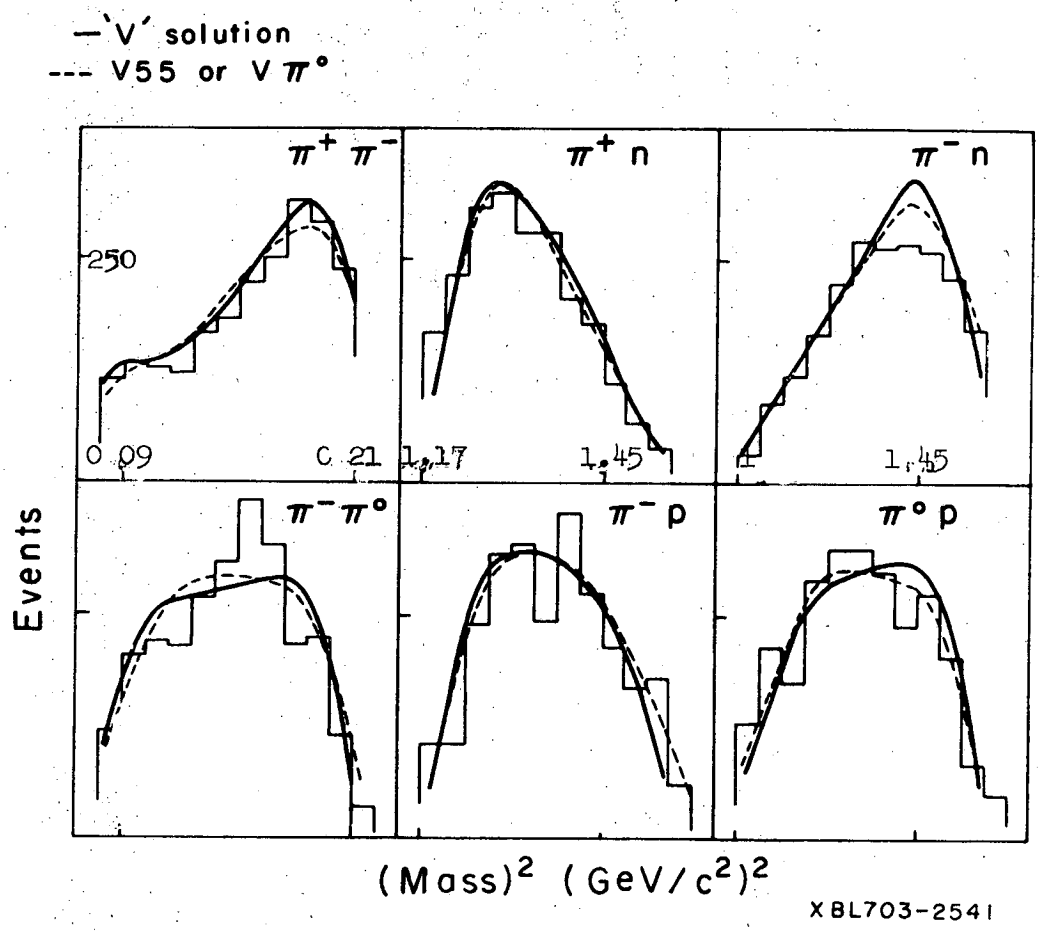
—'V' solution
--- V55 or V π°
π⁺ π⁻
π⁺ n
π⁻ n
250
0.09
0.21
1.17
1.45
1.45
π⁻ π°
π⁻ p
π° p
Events
(Mass)² (GeV/c²)²
XBL703-2541

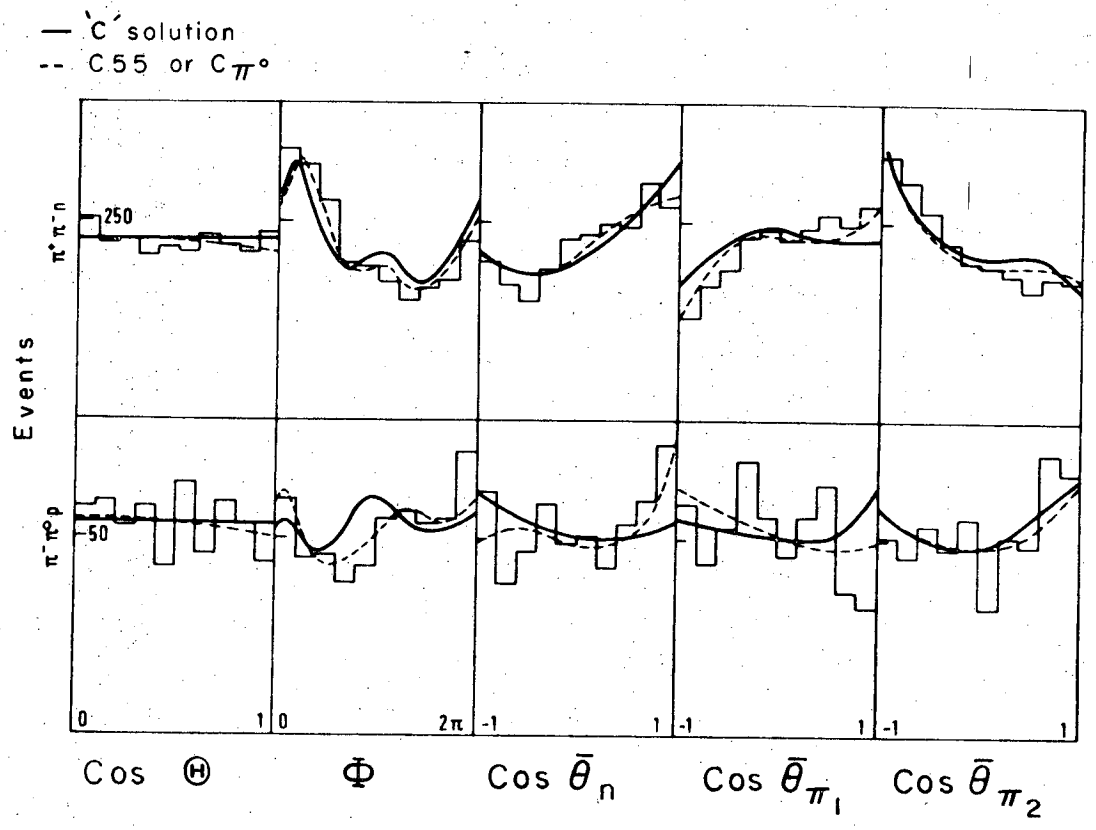
— 'C' solution
-- C55 or Cπ°
Events
π⁺π⁻n
250
π⁻π°p
50
0
1
0
2π
-1
1
-1
1
-1
1
Cos Θ
Φ
Cos θ̄n
Cos θ̄π1
Cos θ̄π2

XBL703-2547

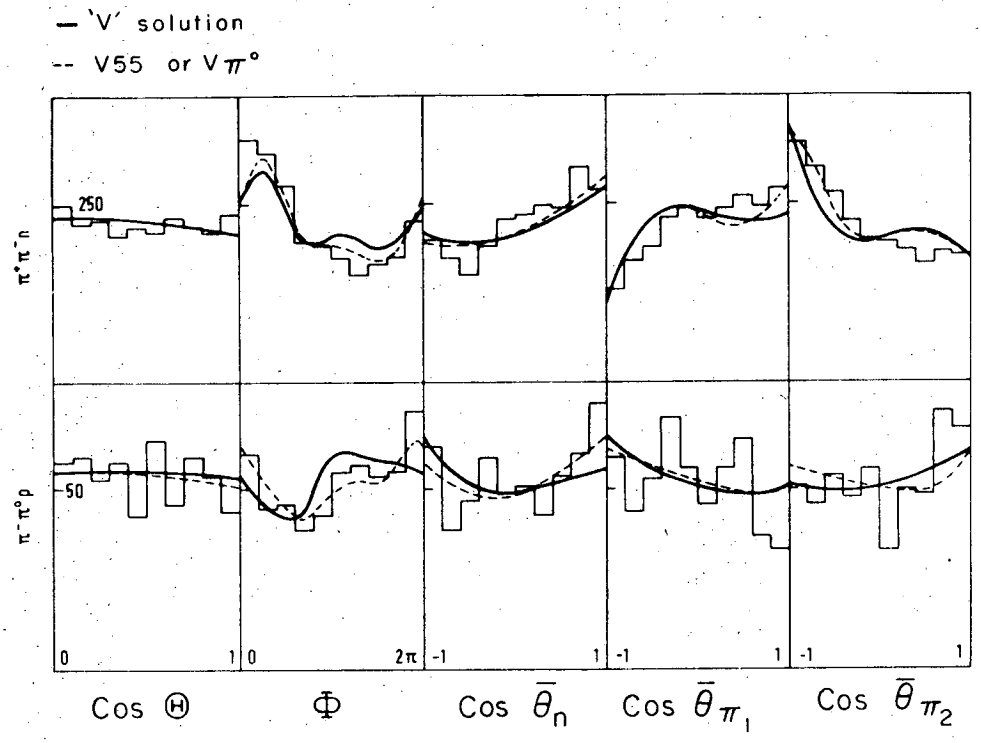
— 'V' solution
-- V55 or Vπ°
250
50
π⁺π⁻n
π⁻π°p
0
1
0
2π
-1
1
-1
1
-1
1
Cos Θ
Φ
Cos θ̄n
Cos θ̄π1
Cos θ̄π2

XBL703-2548

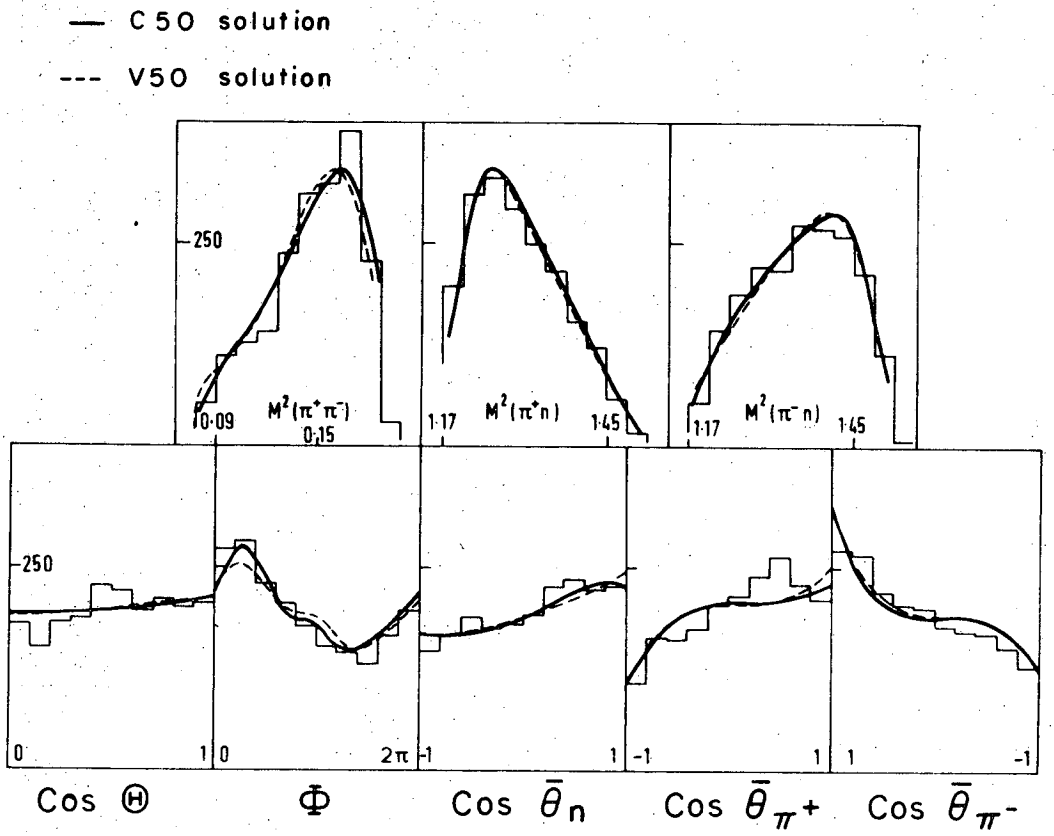
— C 50 solution
--- V50 solution
250
0·09
$M^2(\pi^+\pi^-)$
0·15
1·17
$M^2(\pi^+n)$
1·45
1·17
$M^2(\pi^-n)$
1·45
250
0
1
0
2π
-1
1
-1
1
1
-1
Cos Θ
Φ
Cos $\bar{\theta}_n$
Cos $\bar{\theta}_{\pi^+}$
Cos $\bar{\theta}_{\pi^-}$

XBL703-2539

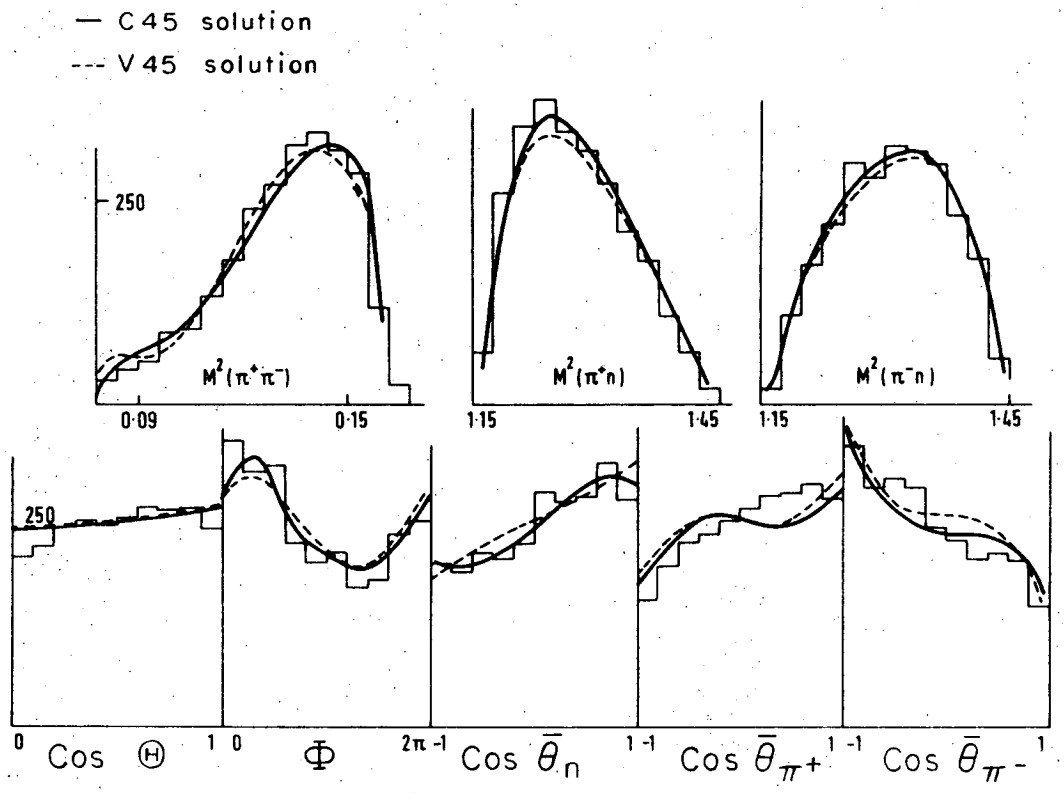
— C45 solution
--- V45 solution
250
$M^2(\pi^+\pi^-)$
0·09
0·15
$M^2(\pi^+n)$
1·15
1·45
$M^2(\pi^-n)$
1·15
1·45
250
0 Cos Θ 1
0 Φ 2π
-1 Cos $\bar{\theta}_n$ 1
-1 Cos $\bar{\theta}_{\pi^+}$ 1
-1 Cos $\bar{\theta}_{\pi^-}$ 1

XBL 703-2546

EXPANSION OF A 2→3 BODY AMPLITUDE
INTO ISOBAR TERMS AND TRIANGLE GRAPHS

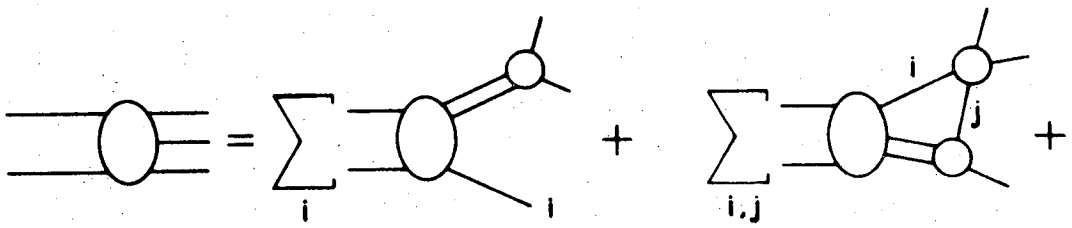

XBL 703-2556

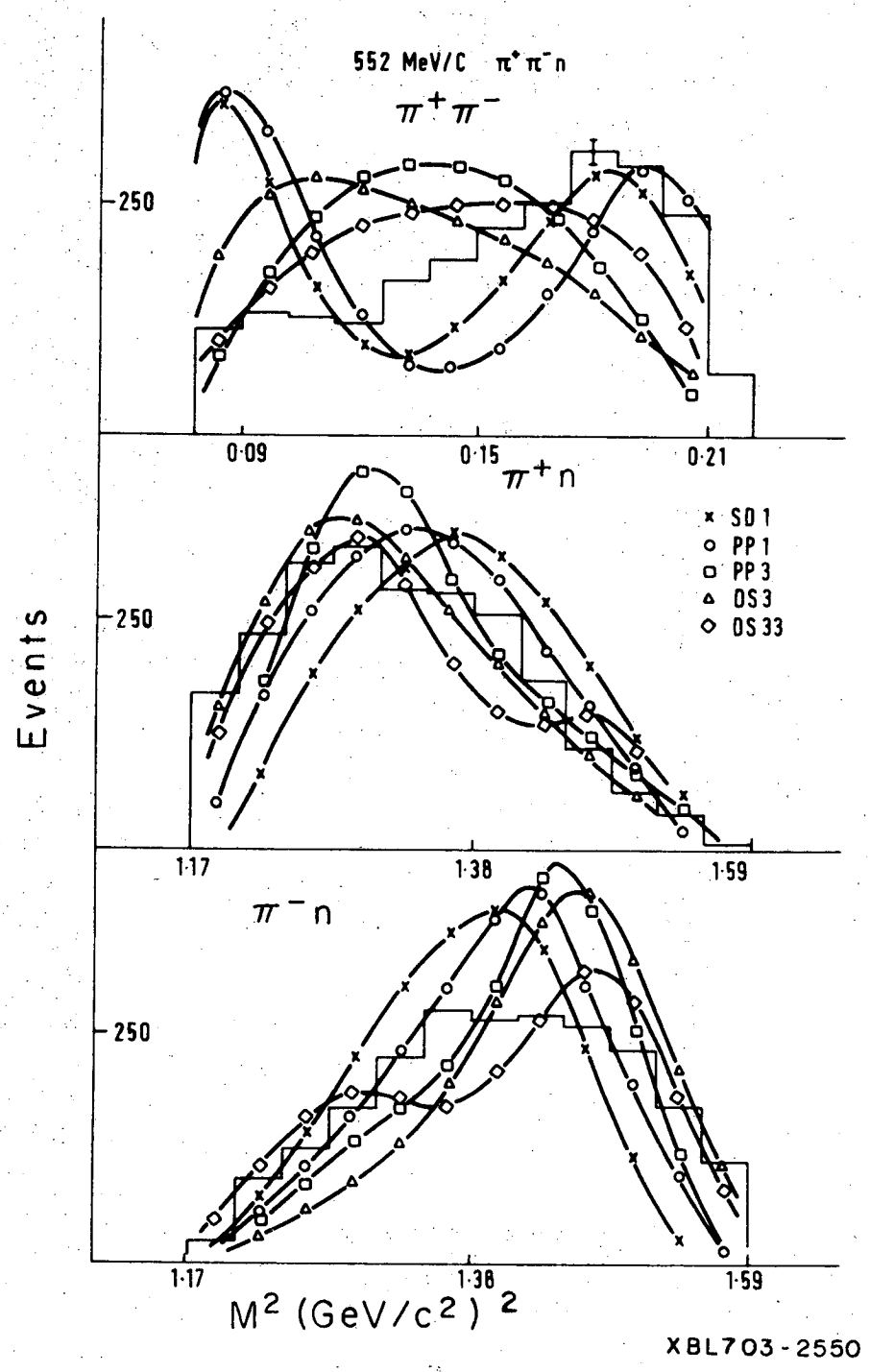
552 MeV/C π⁺π⁻n
π⁺π⁻
250
0·09
0·15
0·21
π⁺n
× SD 1
○ PP 1
□ PP 3
△ DS 3
◇ DS 33
250
1·17
1·38
1·59
π⁻n
250
1·17
1·38
1·59
Events
M² (GeV/c²)²
XBL703-2550

FORMS OF δ_{00} USED

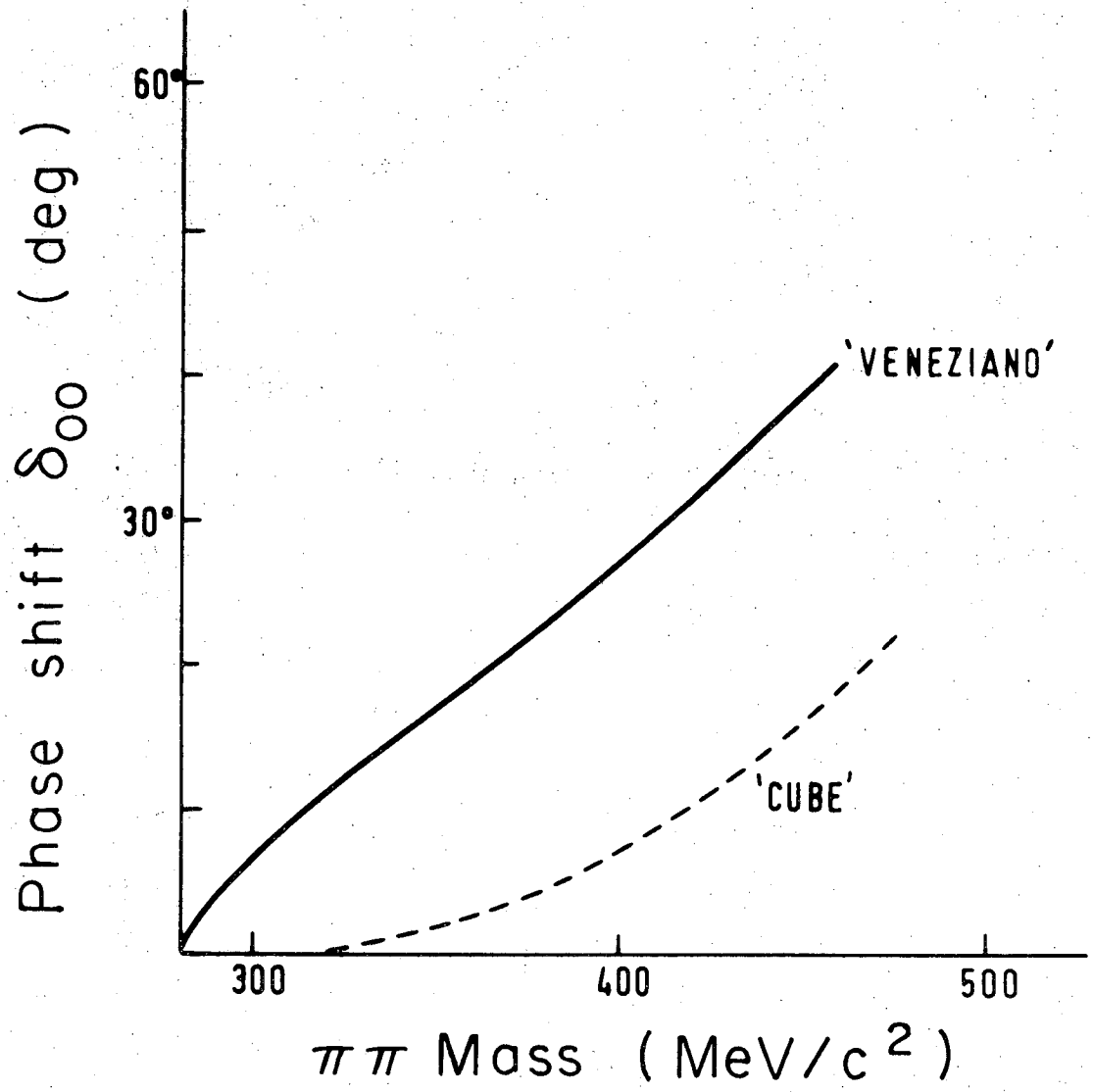

XBL703-2549

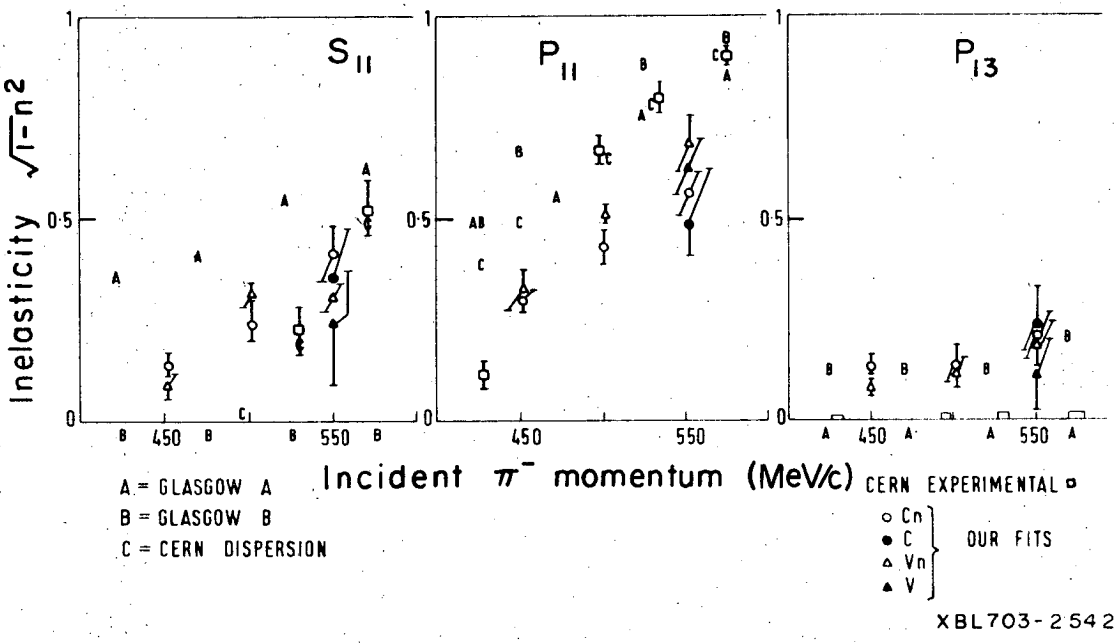
Inelasticity $\sqrt{1-\eta^2}$
S_{11}
P_{11}
P_{13}
1
0·5
0
450
550
Incident π^- momentum (MeV/c)
A = GLASGOW A
B = GLASGOW B
C = CERN DISPERSION
CERN EXPERIMENTAL
Cη
C
Vη
V
OUR FITS
XBL703-2542

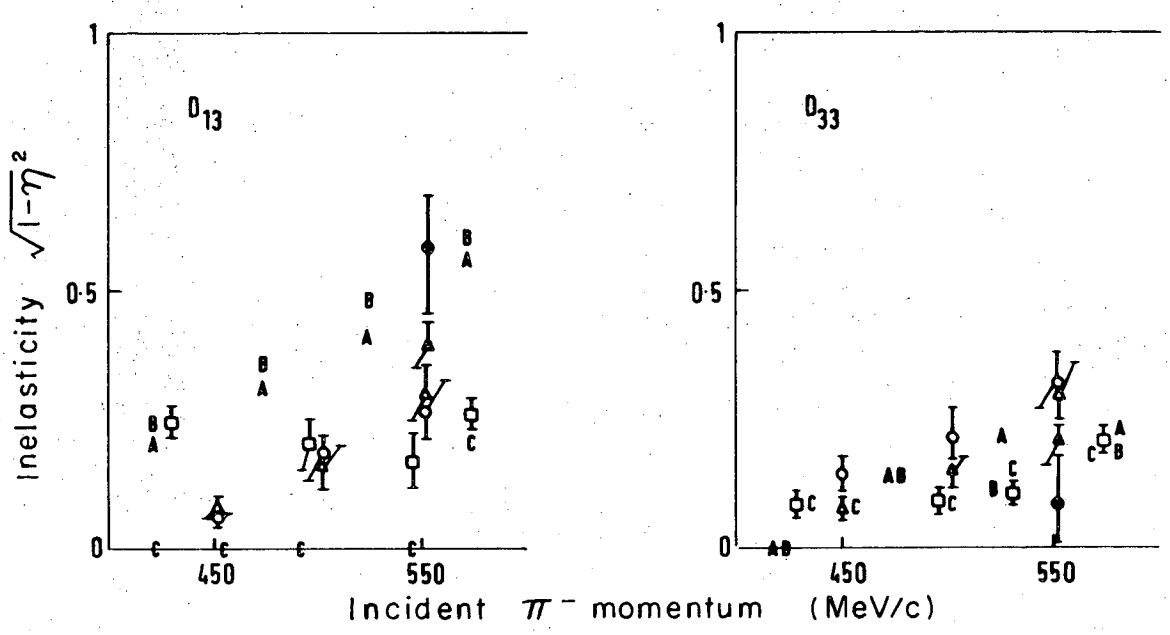
1
0.5
0
D_{13}
D_{33}
Inelasticity $\sqrt{1-\eta^2}$
450
550
Incident π^- momentum (MeV/c)

XBL703-2552

TECHNICAL INFORMATION DIVISION
LAWRENCE RADIATION LABORATORY
UNIVERSITY OF CALIFORNIA
BERKELEY, CALIFORNIA 94720